frontiers | Frontiers in Earth Science

TYPE Original Research
PUBLISHED 26 August 2024
DOI 10.3389/feart.2024.1426525

OPEN ACCESS

EDITED BY
Zhaochong Zhang,
China University of Geosciences, China

REVIEWED BY
Junhong Zhao,
China University of Geosciences
Wuhan, China
Veronica Peverelli,
University of Bologna, Italy

*CORRESPONDENCE
Riccardo Callegari,
riccardo.callegari@geo.uu.se

RECEIVED 01 May 2024
ACCEPTED 26 July 2024
PUBLISHED 26 August 2024

CITATION
Callegari R, Barker AK, Barnes CJ, Walczak K, Ziemniak G, Klonowska I, Kooijman E, Rousku S, Kośmińska K and Majka J (2024) A depleted mantle source for Neoproterozoic continental rifting in the Seve Nappe Complex, Kebnekaise region, northern Swedish Caledonides.
Front. Earth Sci. 12:1426525.
doi: 10.3389/feart.2024.1426525

A depleted mantle source for Neoproterozoic continental rifting in the Seve Nappe Complex, Kebnekaise region, northern Swedish Caledonides

Riccardo Callegari[1,2]*, Abigail K. Barker[1], Christopher J. Barnes[3], Katarzyna Walczak[2], Grzegorz Ziemniak[4], Iwona Klonowska[1], Ellen Kooijman[5], Sabine Rousku[1], Karolina Kośmińska[2] and Jarosław Majka[1,2]

[1]Department of Earth Sciences, Uppsala University, Uppsala, Sweden, [2]Faculty of Geology, Geophysics and Environmental Protection, AGH University of Krakow, Kraków, Poland, [3]Institute of Geological Sciences, Polish Academy of Sciences, Kraków, Poland, [4]Institute of Geological Sciences, University of Wrocław, Wrocław, Poland, [5]Department of Geosciences, Swedish Museum of Natural History, Stockholm, Sweden

The Central Iapetus Magmatic Province (CIMP) is a large igneous province (LIP) emplaced in the Baltican and Laurentian paleocontinents that marks the onset of the Caledonian Wilson Cycle. Paleozoic magmatism of the CIMP is preserved in both northeastern America and northern Europe. This study investigates rocks belonging to the hyper-extended margin of Baltica currently found in the Seve Nappe Complex of the Scandinavian Caledonides. Specifically, U-Pb zircon geochronology and whole-rock geochemistry are applied to a migmatitic variety of the Vierručohkka amphibolite of the Mårma Terrane, to the Aurek gabbro, and amphibolite of the Aurek Assemblage exposed in the Seve Nappe Complex in the Kebnekaise region, northern Swedish Caledonides. U-Pb zircon geochronology yields crystallization ages of 626 $\pm$ 7 Ma for the protolith of the Vierručohkka amphibolite, and 614 $\pm$ 2 Ma and 609 $\pm$ 1 Ma for the emplacement of the Aurek gabbro and amphibolite protolith, respectively. A younger age of 599 $\pm$ 3 Ma is recorded in the Vierručohkka amphibolite and is interpreted as the age of partial melting and migmatization. The geochemical signatures of the rocks demonstrate crustal assimilation during the emplacement of their protoliths and modification due to prograde metamorphic processes during Caledonian subduction. The Vierručohkka amphibolite and the Aurek Assemblage samples display upper and lower crustal assimilation, respectively. Trace elements (Dy, Sm, Lu, and Y) record the growth of metamorphic garnet, while elevated TiO_2 contents record the crystallization of metamorphic rutile. Nevertheless, high field strength elements (HSFE) and ΔNb suggest a depleted mantle source for the magmas of the protoliths of the investigated rocks. Altogether, geochemical data indicate that the igneous activity recorded in the Vierručohkka amphibolite and

the Aurek Assemblage between c. 626–609 Ma is related to continental rifting processes associated with the opening of the Iapetus Ocean.

KEYWORDS

continental rifting, Iapetus Ocean opening, depleted mantle source, crustal assimilation, metamorphic signature

1 Introduction

Understanding continental rifting processes is fundamental to better comprehend the emplacement and the geochemical signatures of large igneous provinces (LIPs) which are extensively studied because of the connection with large scale geological processes (i.e., continental break-up) and their impact on the environment (i.e., mass extension; e.g., Burke and Dewey, 1973; Wignall, 2001). This study focuses on the geochemical signatures of meta-igneous rocks that potentially record a part of the Neoproterozoic continental rifting due to break-up of Rodinia. The break-up of the supercontinent Rodinia was followed by the opening of the Iapetus, Rheic and Tornquist oceans (e.g., Harland and Gayer, 1972; McKerrow and Ziegler, 1972). The opening of the Iapetus Ocean is associated with the emplacement of the Central Iapetus Magmatic Province (CIMP), a large igneous province (LIP) which is exposed in northwestern Europe and northeastern America (Ernst and Bell, 2010; Tegner et al., 2019). In Laurentia, the oldest magmatism related to the CIMP ranges between c. 615–590 Ma (e.g., Kamo et al., 1989; Kamo et al., 1995). A younger event c. 565–550 Ma shows affinities with enriched mantle and depleted upper mantle which is interpreted as being indicative of deep melts of a mantle plume and a second stage of rifting (e.g., Cawood and Nemchin, 2001; Puffer, 2002; Chew and Van Staal, 2014). In northern Europe, metamorphosed igneous and volcanic rocks belonging to the CIMP are found within imbricated nappes of the Scandinavian Caledonides (e.g., Gee et al., 2008; Andersen et al., 2012; Gee et al., 2013; Jakob et al., 2017). Geochronology of these Neoproterozoic mafic dykes yields ages between 616–595 Ma (e.g., Bingen et al., 1998; Svenningsen, 2001; Baird et al., 2014; Gee et al., 2016; Kumpulainen et al., 2016; Kjøll et al., 2019; Tegner et al., 2019). Evidence of the Rodinia break-up and the emplacement of the CIMP are well preserved in the northern part of the Seve Nappe Complex of the Middle Allochthon in the Scandinavia Caledonides (e.g., Tegner et al., 2019). Specifically, this nappe is defined as the outermost Baltica margin representing an ideal region to investigate break-up and CIMP related processes. Moreover, emplacement of the dyke swarm into the hyper-extended Baltoscandian margin triggered a poorly understood high temperature metamorphism which caused partial melting of different lithologies (e.g., Barnes et al., 2019; Kjøll et al., 2019; Walczak et al., 2022). In this study, U-Pb zircon geochronology and bulk-rock geochemistry are applied to a range of lithologies belonging to a migmatitic variety of the Vierručohkka amphibolite and to the Aurek Assemblage of the Mårma Terrane in the Seve Nappe Complex (Figure 1, 2). The main goals are to characterize the crystallization age of the mafic protoliths and to understand their source, crustal assimilation signature, and metamorphism. Furthermore, this work aims to compare the geochemical data obtained for the central-north Scandinavian Caledonides with the Laurentian equivalents, such as mafic dykes in Appalachia (United States; Bédard and Stevenson, 1995; Camiré et al., 1995; Dennis et al., 2004) and a Cenozoic rifting example from the Basin and Range Province of the USA (Dungan et al., 1986). These new data are fundamental for the reconstruction of the still poorly-understood mantle-driven rifting process and subsequent opening of the Iapetus Ocean and offer a means by which to understand not only the source composition of magmatism, but also the heterogeneity of the mantle source that characterizes the dyke swarms in the Scandinavian Caledonides related to the emplacement of the CIMP.

2 Geological setting

The Scandinavian Caledonides preserve a record of the opening, then closure, of the Iapetus Ocean, leading to continental collision between Laurentia and Baltica in the Silurian (e.g., Gee, 1975; Gee et al., 2013). The Caledonides are composed of several allochthons bounded by crustal-scale thrusts (Gee et al., 1985; Gee et al., 2008; Figure 1). The basement of the Caledonides is formed by the Autochthon, or the Baltican paleocontinent. The Parautochthon and Lower Allochthon, derived from the crystalline Baltican basement and its sedimentary cover, respectively, are thrust over the Autochthonous Baltican basement. The Middle Allochthon is interpreted to be composed of the hyper-extended outermost margin of the Baltican continent, including the continent-ocean transition zone (Gee et al., 2020). The Upper Allochthon is thought to be made up of terranes having Iapetus Ocean affinities (i.e., ophiolites, island arc, and back-arc basins rocks; e.g., Stephens, 2020). The Uppermost Allochthon is composed of terranes from the peri-Laurentian continental margin (e.g., Roberts et al., 2007; Corfu et al., 2014).

2.1 The Seve Nappe Complex in the Scandinavian Caledonides

The Seve Nappe Complex (SNC) of the Middle Allochthon is comprised of metasedimentary and metaigneous rocks representing the hyper-extended passive margin of Baltica that was subducted to mantle depths during Iapetus Ocean closure (e.g., Stephens and Gee, 1989; Andréasson, 1994; Gee et al., 2020). The Seve Nappe Complex is commonly divided into three major tectonic units: Lower, Middle and Upper Seve nappes. The Lower and Middle Seve units preserve evidence of high-to ultra-high pressure ((U)HP) metamorphic conditions, including eclogite,

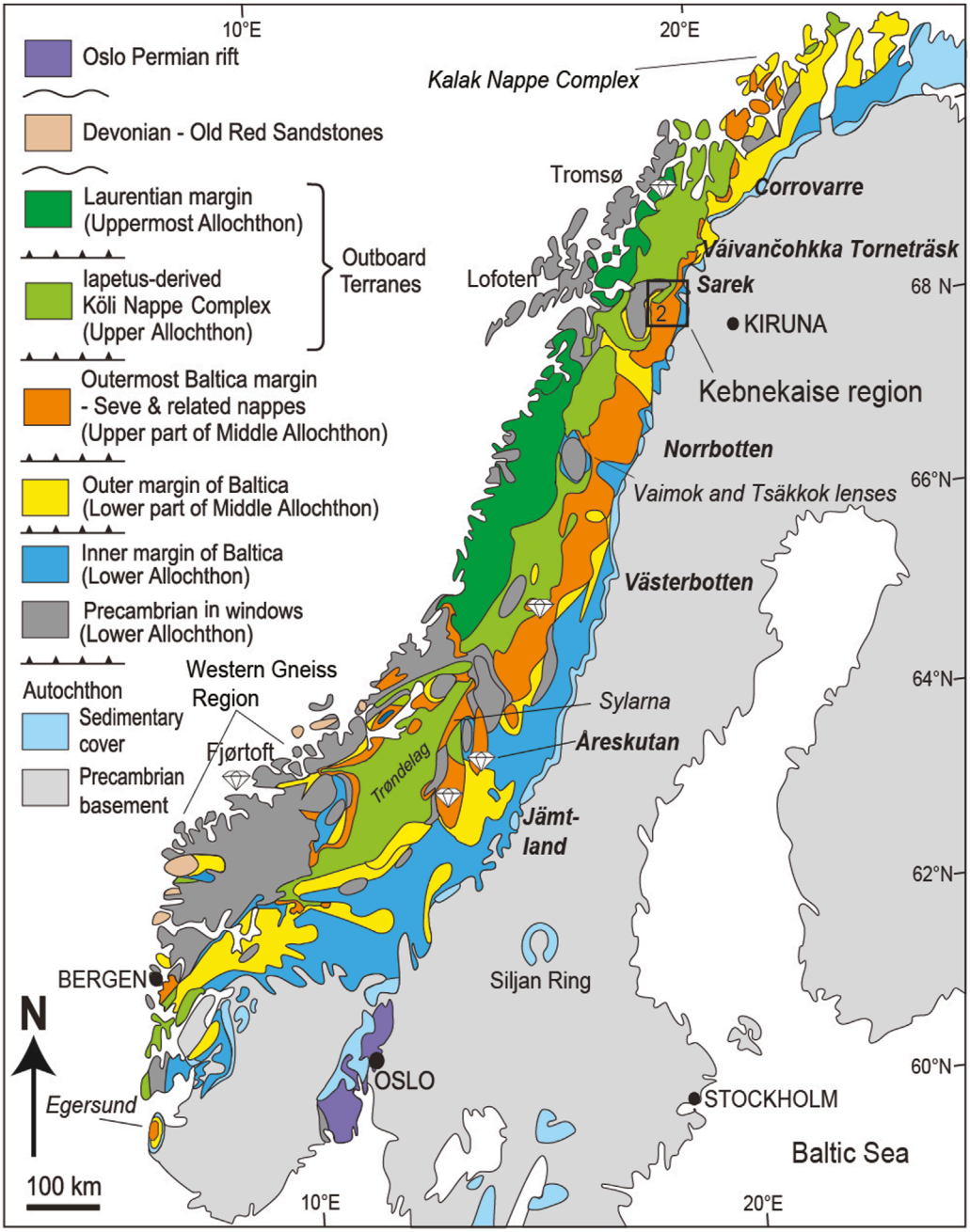

FIGURE 1
Simplified tectonostratigraphic map of the Scandinavian Caledonides, modified from Klonowska et al. (2016), Gee et al. (2016). The study area is marked with a black box. Diamonds indicate the discovery of micro-diamonds inclusions in UHP terrain.

garnet peridotite, and diamond-bearing gneiss (e.g., Janák et al., 2013; Majka et al., 2014; Gilio et al., 2015; Klonowska et al., 2017; Bukała et al., 2018; Petrík et al., 2019; Fassmer et al., 2021). In the northern Scandinavian Caledonides, the (U)HP character of the metamorphism apparently decreases from southwest to northeast until it is no longer found in the north (e.g., Walczak et al., 2022; Barnes et al., 2023). The Upper Seve nappe consists of sandstones and carbonates and hosts a widespread dolerite dyke swarm (e.g., Stølen, 1994; Svenningsen, 1994).

2.1.1 The Neoproterozoic dyke swarm in the Middle Allochthon

Late Neoproterozoic dykes are exposed in southwestern Norway (Egersund area; e.g., Bingen et al., 1998), and in the Middle and Upper Allochthons of the Scandinavian Caledonides (e.g., Kjøll et al., 2019; Tegner et al., 2019). This dyke swarm has been referred to in different ways, such as the Baltoscandian Dyke Swarm (Andréasson, 1994), the Baltoscandian margin dyke swarm (Svenningsen, 1994) and the Scandinavian Dyke Complex

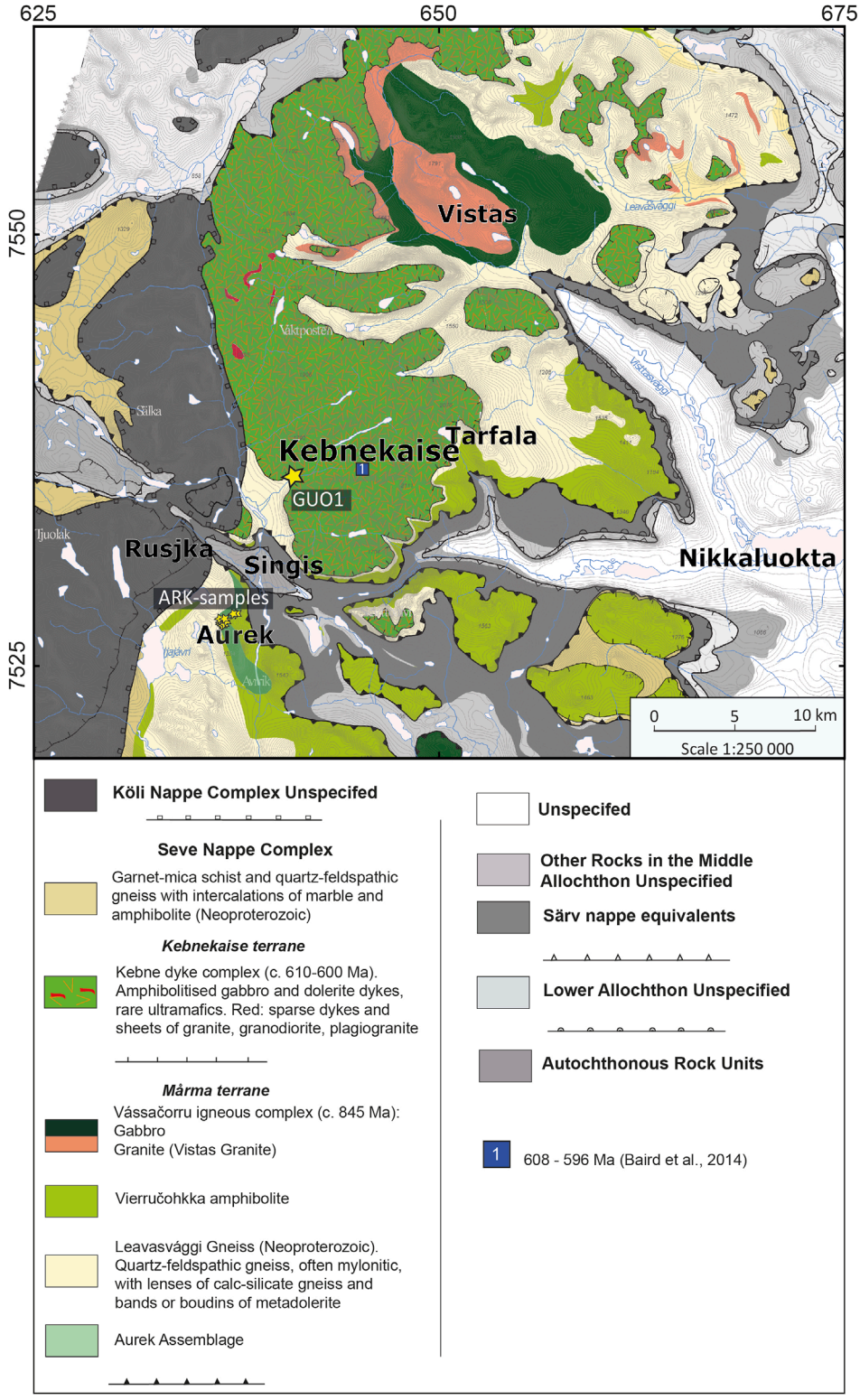

FIGURE 2
Geological map of the Kebnekaise Mts. area (after Callegari et al., 2023; Thelander, 2009). Sample localities are marked by yellow stars.

(Tegner et al., 2019). In this work, the term Baltoscandian Dyke Swarm is applied. The Baltoscandian Dyke Swarm in the Egersund area is denoted as the Egersund Dyke Swarm and it yielded an age of c. 616 Ma (Bingen et al., 1998). In the central portion of the orogen in the Särv Nappe of the Middle Allochthon it is referred as the Ottfjället dyke swarm (e.g., Hollocher et al., 2007), and Sarek Dyke

Complex, and Kebne Dyke Complex in the north part of the Seve Nappe Complex (e.g., Svenningsen, 2001; Baird et al., 2014). The Baltoscandian Dyke Swarm extends into northern Norway in the Indre Troms and Corrovarre areas (e.g., Roberts, 1990; Zwaan and Van Roermund, 1990; Stølen, 1994). In the Seve Nappe Complex, the intrusive ages of the Baltoscandian Dyke Swarm are reported to be c. 608 Ma for the Sarek Dyke Swarm (e.g., Svenningsen, 2001; Root and Corfu, 2012). The Kebne Dyke Complex yielded various intrusive ages such as c. 605 Ma (e.g., Paulsson and Andréasson, 2002), c. 608–596 Ma (Baird et al., 2014), and c. 578 Ma (Kirsch and Svenningsen, 2016). In addition to the dyke swarms in the Seve Nappe Complex/Middle Allochthon, protoliths of various eclogites, metadolerites, and amphibolites, which formed during Cambrian–Ordovician subduction and exhumation, are also thought to belong to the CIMP (e.g., Andréasson and Albrecht, 1995). The Vierručohkka amphibolite and the Aurek Assemblage of the Seve Nappe Complex in the Kebnekaise region are part of these hypothesized overprinted products of the Neoproterozoic rifting.

2.2 The Seve Nappe Complex in the Kebnekaise region

The Seve Nappe Complex in the studied area includes the Kebnekaise and Mårma terranes. The Kebnekaise Terrane is composed of the Kebne Dyke Complex (Baird et al., 2014). The Kebne Dyke Complex is characterized by a T-MORB affinity (e.g., Baird et al., 2014). It is constituted of amphibolites and rare felsic rocks along with minor ultramafic and gabbroic rocks. The Mårma Terrane extends to the eastern part of the Kebnekaise mountains. It is composed of the Vássačorru Igneous Complex (VIC), Vierručohkka amphibolite (VA), the Leavasvággi gneiss, and the Aurek Assemblage (Figure 2; e.g., Thelander, 2009; Andreásson et al., 2018). The VIC is a bimodal igneous complex mainly comprised of granite, dolerite, and gabbro. Emplacement ages range between c. 865–829 Ma (e.g., Paulson and Andréasson, 2002; Jakob et al., 2022; Callegari et al., 2023). The VA was previously interpreted as part of the Kebne Dyke Complex (e.g., Paulsson and Andréasson, 2002) but this hypothesis has been called into question by later studies, due to varied geochemical signatures showing affinities with both N-MORB and E-MORB compositions (e.g., Andréasson et al., 2018). The Leavasvággi gneiss is described as a mylonitic, locally migmatitic, paragneiss. A variety of this mylonitic paragneiss is referred to as the Storglaciären gneiss. However, recent investigation of this unit found that at least a portion of this mylonitic gneiss is an unequivocal orthogneiss, and its protolith is part of the VIC (Callegari et al., 2023). The Aurek Assemblage is composed of the Aurek gabbro, the Aurek amphibolite, and the Vidja gneiss (Tilke, 1986). In the Kebnekaise region, lenses of Aurek gabbro are separated from the surrounding Vidja gneiss by the Aurek amphibolite; collectively, the Aurek gabbro and amphibolite have been interpreted to be a smaller magmatic body related to the VIC (Tilke, 1986). However, their crystallization age is much younger, with known ages ranging between c. 615–610 Ma (Rousku et al., 2021). For this reason, we maintain designation of the Aurek Assemblage as a separate unit (Figure 2).

3 Methods

3.1 Mineral chemistry

Mineral chemistry in the samples was determined using wavelength dispersive spectroscopy (WDS) with a Jeol JXA8530F Hyperprobe Field Emission Electron Probe Microanalyzer (EPMA) at the Department of Earth Sciences, Uppsala University, Sweden and with a Jeol JXA-8230 SuperProbe EPMA at the Faculty of Geology, Geophysics and Environment Protection, AGH University of Krakow, Poland. Natural and synthetic standards were used for calibration. Operating conditions used for WDS were as follows: 10 nA beam current, 15 kV accelerating voltage, and counting times of 10 s on peak and 5 s for background positions at Uppsala University, and 15 nA beam current, 15 kV accelerating voltage, and counting times of 20 s on peak and 10 s for each offset at AGH University of Krakow. The EPMA was also used to obtain X-ray maps for the composition of garnet for Si, Ti, Al, Fe, Mg, Mn, Ca, Na, K, Y, P and Ce with an accelerating voltage of 15 kV, a beam current of 100 nA, a dwell time of 100 ms and pixel size of 2 µm. Maps were processed using the XMapTools 3 software (Lanari et al., 2019).

3.2 Bulk rock geochemistry

Bulk rock geochemistry was conducted for the banded amphibolite and Aurek Assemblage rocks. Bulk rock analysis was performed at Mineral Laboratories (Bureau Veritas) in Canada. The rocks were pulverized and fused with lithium metaborate [$LiBO_2$] and lithium tetraborate [$Li_2B_4O_7$]. Major elemental concentrations were measured via inductively coupled plasma emission spectroscopy (ICP-ES). Trace element concentrations were measured via inductively coupled plasma mass spectrometry (ICP-MS). The internal standard used for major elements analysis is SO-19, (n = 4), with record reproducibility of <3% (2 s.d.), while for trace element analysis the standard is OREA30A with a reproducibility of 10%–20% (2 s.d.). The detection limits (wt%) of all major oxides are 0.01, except for Cr_2O_3 at 0.002 and Fe_2O_3 with 0.04. Detection limits for trace elements are as follows: V: 8.0 ppm; Ba, Be, Sn and Sc: 1.0 ppm; Ga, Sr and W: 0.5 ppm; Nd: 0.3 ppm; Co. and Th: 0.2 ppm; Cs, Hf, Nb, Rb, Ta, U, Zr, Y, La and Ce: 0.1 ppm; Sm, Gd, Dy and Yb: 0.05 ppm; Er: 0.03 ppm; Ho, Pr and Eu: 0.02 ppm; Tb, Tm and Lu: 0.01 ppm. The software package GCDkit 6.0 was used to plot the geochemical diagrams (Janák et al., 2012).

3.3 Zircon U/Pb geochronology and trace elements

Zircon grains were dated both *in situ* in thin section for sample GUO1 and as separates mounted in epoxy for samples ARK13 and ARK11. For *in situ* analysis, back-scattered electron (BSE) images were acquired using the JEOL Superprobe EPMA at AGH University of Krakow. For epoxy mounts, the zircon grains were hand-picked after crushing, sieving, and Frantz magnetic separation at the Institute of Geological Sciences, Polish Academy of Sciences in Kraków, Poland. Zircons were mounted at the Vegacenter, Swedish Museum of Natural History, Stockholm, Sweden, and imaged with BSE

and cathodoluminescence (CL) using the Jeol JXA8530F EPMA at Uppsala University. Obtained images were used for the selection of the analytical spots for both dating and rare earth element (REE) analyses. U-Pb isotope analyses and REE analyses for both the *in situ* grains and zircon separates were conducted using an ESI NWR193 ArF excimer laser ablation system at the Vegacenter. A Nu Plasma II multi collector inductively coupled plasma mass spectrometer (MC-ICP-MS) connected to the laser ablation system was adopted for *in situ* U-Pb geochronology. The mass-to-charge ratio (m/z) corresponding to masses 202, 204, 206, 207 and 208 were measured on ion counters and those corresponding to 232, 235, 238 were measured on Faraday collectors. The beam diameter ranged from 15 to 20 μm for ablation with a frequency of 7 Hz and a laser fluence of 2 J/cm^2. Helium was used as a sample carrier gas (0.45 L/min) mixed with argon (mixed flow rate 0.8 L/min). Analytical runs had a washout time of 20 s, ablation time of 20 s, and integration time of 0.5 s.

REE, Zr, U, and Th were collected using an AttoM high resolution inductively coupled plasma mass spectrometer (HR-ICP-MS). The laser had a beam diameter of 20 μm for ablation with a frequency of 8 Hz and a laser fluence of 3.7 J/cm^2. Helium was used as a sample carrier gas (0.45 L/min) mixed with argon (mixed flow rate 0.9 L/min). The adopted primary reference, both for U-Pb geochronology and trace elements, was 91500 zircon (1,065 Ma; Wiedenbeck et al., 2004). The GJ-1 zircon (609 Ma; Jackson et al., 2004), Plešovice zircon (337 Ma; Sláma et al., 2008) and Temora 2 zircon (417 Ma; Black et al., 2004) were used as secondary reference materials. U-Pb zircon results were plotted using the software IsoplotR (Vermeesch, 2018).

4 Results

4.1 Petrography and mineral chemistry

This study focuses on three subunits of the Mårma terrane of the Seve Nappe Complex in the Kebnekaise region: banded amphibolites of the Vierručohkka amphibolite, the Aurek gabbro, and Aurek amphibolite (Figure 2). Fourteen samples were selected for petrographic description and geochemical analysis; of the fourteen samples, based on petrography and microstructures three were selected for U-Pb zircon geochronology. For the Vierručohkka amphibolite, a sample of the banded amphibolite was selected. Two representative samples of the Aurek metagabbro were chosen for the petrographic description and mineral characterization, one of which was chosen for U-Pb zircon geochronology. Two Aurek amphibolite samples were selected for the petrographic description and mineral characterization, one of which was selected for U-Pb zircon geochronology. The complete list of all the samples can be found in Supplementary Table S1. All mineral abbreviation are after Whitney and Evans (2010).

4.1.1 Vierručohkka banded amphibolite

At the outcrop scale, the Vierručohkka banded amphibolites have a migmatitic fabric with alternating melanocratic and leucocratic layers (Supplementary Figure S1). The melanocratic layers are composed of amphibole + titanite + quartz + plagioclase ± muscovite ± biotite (Figure 3A). The leucocratic layers consist of garnet + plagioclase + quartz + titanite + epidote group minerals (Figure 3B). Zircon is present as an accessory phase. Amphibole is calcic according to the classification of Hawthorne et al. (2012). The composition varies between pargasite and Fe-pargasite (Si = 6.35–6.52 atoms per unit formula; apfu). The X_{Fe} number ($Fe^{2+}/Mg+Fe^{2+}$) ranges from 0.48 to 0.51 (see Table 1). Two different types of symplectite along the amphibole grain boundaries are visible at thin section scale. The first is formed by plagioclase + clinozoisite (Figure 3C), and the second is composed of quartz + zoisite (Figure 3D). Garnet occurs as euhedral grains in the leucocratic layer only, with diameter sizes ranging between c. 130–710 μm (average of 465 μm). Garnet is not fractured and hosts inclusions of quartz, epidote, and plagioclase (Figures 3E, F). Garnet X-ray maps reveal that the almandine content is higher in the core and decreases slightly toward the rim whereas the grossular component increases toward the rim (Supplementary Figure S1). The pyrope and spessartine trends are relatively flat throughout the grain. Representative garnet cores have the composition X_{Alm} ($Fe^{2+}/(Fe^{2+} + Mg + Ca + Mn)$) = 0.50, X_{Grs} ($Ca/(Fe^{2+} + Mg + Ca + Mn)$) = 0.35, X_{Prp} ($Mg/(Fe^{2+} + Mg + Ca + Mn)$) = 0.07, and X_{Sps} ($Mn/(Fe^{2+} + Mg + Ca + Mn)$) = 0.08. The rims have X_{Alm} = 0.47, X_{Grs} = 0.37, X_{Prp} = 0.08, and X_{Sps} = 0.08 (Table 1). Plagioclase occurs both within the melanocratic and leucocratic layers (Figures 3B, C). The composition does not change much between the textural position, resulting in a representative composition of X_{Ab} ($Na/(Na + Ca + K)$) = 0.59, X_{An} ($Ca/(Na + Ca + K)$) = 0.40, and X_{Or} ($K/(Na + Ca + K)$) = 0.01 with a maximum of X_{Ab} = 0.62 and a minimum of X_{Ab} = 0.58 (Table 1). Micas are very scarce; muscovite and biotite are located within the melanocratic layers as elongate crystals aligned parallel to amphibole elongation. The muscovite is characterized by Si = 3.2 apfu and biotite by a X_{Fe} ($Fe^{2+}/(Fe^{2+}+ Mg)$) = 0.41 (Table 1). Titanite is widespread within both layers. Occasionally clinozoisite forms coronas around titanite grains. Importantly, textures indicating crystallization in the presence of a melt phase were recognized. In particular, pseudomorphs of melt, such as quartz films around garnet grain boundaries and melt pools were found (Figures 3G, H), which correspond to the growth of crystal from a melt and infiltration of the former melt along grain boundaries respectively (Sawyer, 2001; Vernon, 2011).

4.1.2 Aurek gabbro

The representative mineral composition of the Aurek gabbro is garnet + orthopyroxene + clinopyroxene + amphibole + plagioclase + rutile + kyanite ± zoisite. Zircon is present as an accessory phase. Clinopyroxene is classified as augite with a representative composition of X_{En} ($Mg/(Mg +Fe^{2+} + Ca + Mn)$) = 0.37, X_{Wo} ($Ca/(Ca + Mn + Mg + Fe^{2+})$) = 0.28, X_{Fs} ($(Fe^{2+} + Mn)/(Fe^{2+} + Mn + Ca + Mg)$) = 0.34, X_{Ac} ($Na/(Na + Fe^{2+} + Mn + Mg + Ca)$) = 0.01 (Table 2), and is replaced by amphibole and orthopyroxene (Morimoto et al., 1988). Orthopyroxene is surrounded by amphibole and coronitic garnet (Figure 4A). Amphibole classification varies from Mg-hornblende (Si = 7.13) to pargasite (Si = 6.89) (Hawthorne et al., 2012), the X_{Fe} ranges between 0.19 and 0.36 and amphiboles show exsolution of kyanite and zoisite. Garnet does not show chemical zoning and forms coronae around orthopyroxene and amphibole (Figure 4A). Garnet compositions are in the range of X_{Alm} = 0.44–0.59, X_{Prp} = 0.24–0.15, X_{Grs} = 0.30–0.22, and X_{Sps} = 0.01–0.03. Furthermore, plagioclase compositions range between X_{Ab} = 0.39–0.48, X_{An} =

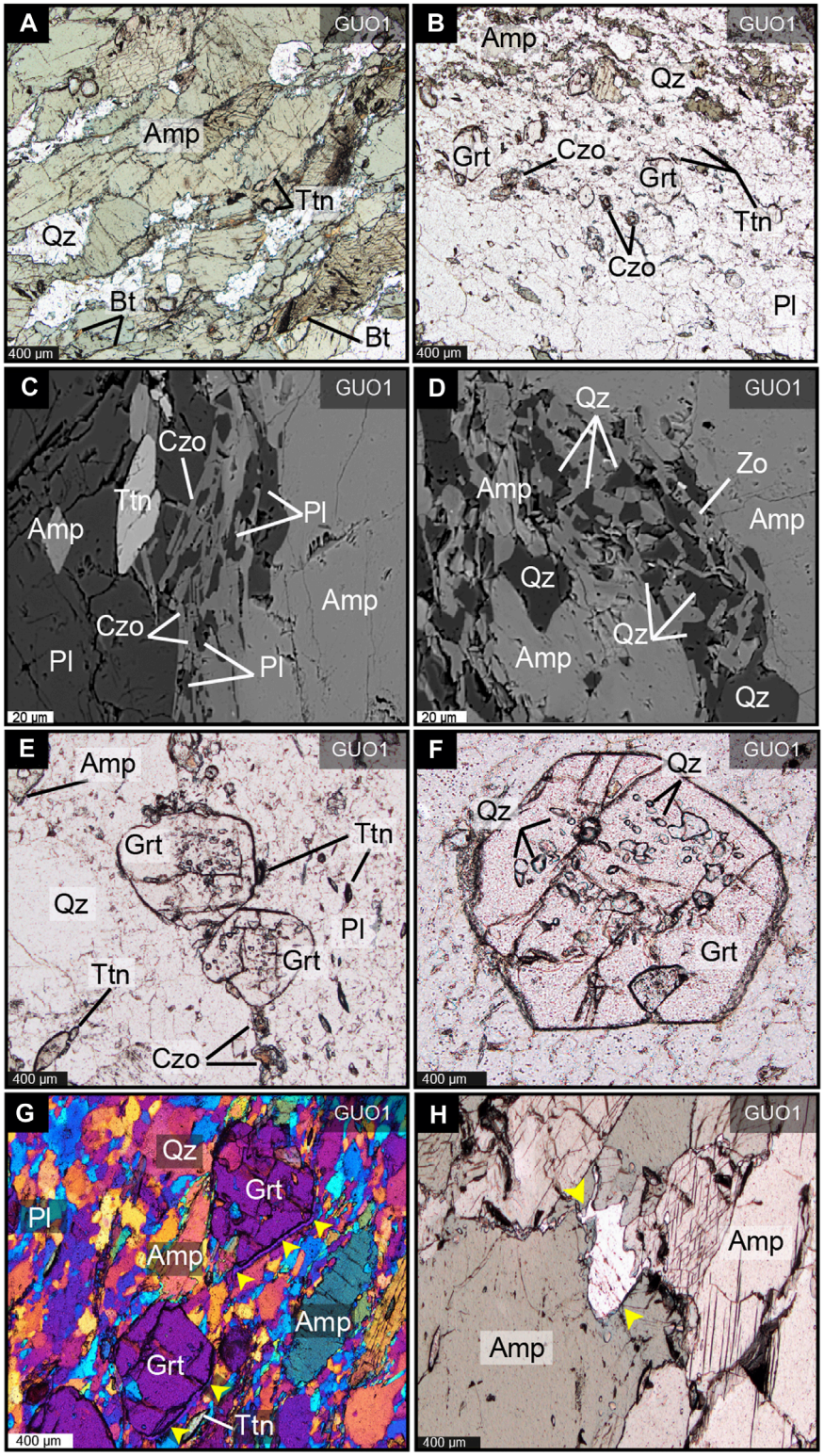

FIGURE 3
Photomicrographs and BSE images of the Vierručohkka banded amphibolite rock (GUO1). **(A)** Amphibole-bearing layer composed of amphibole + quartz + biotite + titanite; PPL. **(B)** Garnet-bearing layer composed of garnet + quartz + plagioclase + titanite + clinozoisite; PPL. **(C, D)** BSE images of symplectite at the amphibole boundary; **(C)** plagioclase + clinozoisite, **(D)** quartz + zoisite. **(E)** Magnification of garnet grain; CPL. **(F)** Garnet hosts quartz inclusions; PPL. **(G)** Auxiliary quartz-plate CPL photomicrograph of melt film around garnet (yellow arrows). **(H)** Melt pods indicated by yellow arrows. CPL, cross polarized light; PPL, plane polarized light; BSE, electron backscattered.

10.3389/feart.2024.1426525

TABLE 1 Representative EPMA data of the banded amphibolite (GUO1). Formulae based on 12 oxygens (garnet), 24 oxygens (amphibole), 11 oxygens (micas) and 8 oxygens (plagioclase). Oxides are expressed in wt%, cations in a.p.f.u.

GUO1	Grt core	Grt core	Grt rim	Grt rim	Prg	Prg	Fe-Prg	Pl	Pl	Bt	Ms
SiO_2	37.92	38.35	38.42	38.48	43.43	43.83	42.55	62.48	64.03	37.26	47.23
TiO_2	0.16	0.14	0.05	0.10	0.14	0.77	0.75	0.00	0.04	1.65	1.15
Al_2O_3	20.81	21.37	21.33	21.27	13.82	13.92	14.03	23.88	23.18	16.84	31.75
Cr_2O_3	0.00	0.00	0.00	0.06	0.00	0.07	0.07	0.00	0.00	0.19	0.22
FeO	22.85	22.83	21.69	21.90	16.34	15.73	16.50	0.01	0.02	15.58	1.57
MnO	3.81	3.76	3.15	3.54	0.25	0.25	0.21	0.00	0.00	0.12	0.02
MgO	1.94	2.01	1.94	1.95	9.24	9.41	8.77	0.00	0.00	12.77	1.66
CaO	12.50	12.38	13.41	13.79	11.45	11.47	11.66	5.36	4.50	0.13	0.06
BaO	nd	nd	nd	nd	nd	nd	nd	0.00	0.00	0.46	1.20
Na_2O	0.01	0.03	0.07	0.00	1.72	1.72	1.77	8.26	8.31	0.05	0.63
K_2O	0.03	0.00	0.00	0.00	0.91	0.97	1.02	0.14	0.06	9.12	9.64
Total	100.03	100.87	100.06	101.09	97.29	98.14	97.34	100.13	100.14	94.16	95.14
Si	3.003	3.003	3.018	2.999	6.465	6.483	6.395	2.814	2.746	2.820	3.174
Ti	0.009	0.008	0.003	0.006	0.079	0.086	0.085	0.001	0.000	0.094	0.058
Al	1.942	1.972	1.974	1.954	2.424	2.427	2.485	1.201	1.237	1.502	2.515
Cr	0.000	0.000	0.000	0.004	0.000	0.009	0.008	0.000	0.000	0.011	0.012
Fe^{2+}	1.513	1.495	1.425	1.428	2.034	1.946	2.074	0.001	0.000	0.986	0.088
Mn	0.256	0.249	0.210	0.234	0.031	0.031	0.027	0.000	0.000	0.007	0.001
Mg	0.229	0.235	0.227	0.227	2.050	2.075	1.965	0.000	0.000	1.441	0.166
Ca	1.060	1.039	1.128	1.152	1.826	1.818	1.878	0.212	0.252	0.011	0.005
Ba	nd	nd	nd	nd	nd	nd	nd	0.000	0.000	0.014	0.032
Na	0.001	0.004	0.011	0.000	0.496	0.493	0.515	0.708	0.704	0.007	0.082
K	0.003	0.000	0.000	0.000	0.172	0.183	0.195	0.003	0.008	0.881	0.826
Total	8.016	8.005	7.995	8.003	15.577	15.551	15.627	4.940	4.948	7.773	6.959
^{X}Alm	0.495	0.495	0.477	0.470							
^{X}Prp	0.075	0.078	0.076	0.075							
^{X}Sps	0.084	0.083	0.070	0.077							
^{X}Grs	0.347	0.344	0.377	0.379							
^{X}Fe					0.498	0.484	0.513			0.406	
^{X}Ab								0.579	0.624		
^{X}An								0.415	0.373		
^{X}Or								0.006	0.003		

0.60–0.52, and X_{Or} = 0.00–0.02 and plagioclase is often replaced by acicular kyanite (Figure 4B).

4.1.3 Aurek amphibolite

The representative mineral assemblage of the Aurek amphibolite is amphibole + clinopyroxene + orthopyroxene + garnet + plagioclase + quartz + kyanite ± rutile ± zoisite. Rare ilmenite and calcite are also present. Zircon is present as an accessory phase. The amphibole composition varies between pargasite (Si = 6.13 apfu) and Mg-hornblende (Si = 7.55 apfu) according to the classification of Hawthorne et al. (2012), and X_{Fe} ranges between 0.19–0.36 (Table 3). The clinopyroxene can be classified as diopside based on the composition of X_{Wo} = 0.47–0.50, X_{En} = 0.43–0.45, X_{Fs} = 0.07–0.08, X_{Ac} = 0.00–0.03 (Morimoto et al., 1988). The X_{Fe} ranges between 0.13 and 0.15 and clinopyroxene is usually replaced by orthopyroxene and titanite. The orthopyroxene has a composition of $En_{68}Fs_{29}Wo_3Ac_0$ (Morimoto et al., 1988), X_{Fe} is 0.29 and it is usually surrounded by amphibole. Garnet can be found in the matrix of the amphibolite and as coronitic garnet around the orthopyroxene (Figures 4C, D). Garnet composition varies between the rim and core. Garnet cores are characterized by X_{Alm} = 0.46, X_{Prp} = 0.28, X_{Grs} = 0.25, X_{Sps} = 0.1, and garnet rims by X_{Alm} = 0.48, X_{Prp} = 0.29, X_{Grs} = 0.22, X_{Sps} = 0.1 (Table 3). Plagioclase shows compositions in the range of X_{Ab} = 0.21–0.31, X_{An} = 0.77–0.68 and X_{Or} = 0.03–0.01. Plagioclase also displays exsolution of kyanite (Figure 4D).

4.2 Bulk rock geochemistry

All the studied samples, despite belonging to different units, show similar trends for major elements (all the analyses are reported in Supplementary Table S2). Trace element geochemistry for the banded amphibolite, Aurek metagabbro and Aurek amphibolite shows elevated and scattered patterns for large-ion lithophile elements (LILE) such as Rb, Ba, and Sr (Figures 5A–C). Rb values range from 1 to 19 ppm, Ba values from 21 to 79 ppm, and Sr shows values between 160 and 291 ppm. The Aurek gabbro and amphibolite display similar LILE contents (Figures 5A–C). Notably, the banded amphibolite records the highest value for Ba (79 ppm), and Y (41 ppm) compositions (Figures 5B, C). In terms of Nd, the majority of the samples plot between 4 and 0.1 ppm, with the two highest values of 7 ppm and 9 ppm recorded by the Aurek gabbro and the banded amphibolite, respectively (Figure 5D). Thorium values range mostly between 0.1 and 2 ppm, although the banded amphibolite does record a high value of 10 ppm (Figure 5E). Scattered La values are present for the Aurek gabbro and amphibolite ranging from 1 to 5 ppm, with the banded amphibolite showing the highest value of 17 ppm (Figure 5F). Dy, Sm, Lu and Y are positively correlated (Figures 6A–C) and TiO_2 shows a positive trend with Y, where three samples from the Aurek gabbro and amphibolite record elevated TiO_2 content (Figure 6D). The primitive mantle normalized multi-elements diagram (Figure 7A) generally shows low values of LILE compared to the lower and upper crust values (Rudnick and Gao, 2003; Figure 7A). The Aurek gabbro and amphibolite, although with a lower concentration of LILE and HFSE, display pronounced peaks of K and Sr, characteristic of a lower crust signature (Figure 7A). The Aurek sample suites have variably pronounced positive Ti anomalies (Figure 7A). The banded amphibolite shows affinity with upper crust values for both LILE and HFSE (Figure 7A). The chondrite normalized REE diagram (Figure 7B) compares the studied samples with MORB values of Kelley et al. (2013), and N-MORB and E-MORB (Sun and McDonough, 1989). The Aurek sample suite displays flat REE patterns with positive Eu anomalies; they are depleted compared to N-MORB and E-MORB (Figure 7B). Moreover, they show comparable values and trends to the depleted MORB from Kelley et al. (2013). The banded amphibolite shows enriched values in all the REE spectra and a negative Eu anomaly (Figure 7B). Specifically, it displays higher values than the N-MORB and E-MORB of Sun and McDonough (1989). Nevertheless, it still plots in the MORB range of Kelley et al. (2013) although in with the more enriched compositions (Figure 7B).

4.3 Zircon U/Pb geochronology and rare earth element composition

The results of the U-Pb zircon geochronology are reported in Supplementary Table S3. Representative high-contrast BSE images of zircon grains are shown in the Supplementary Material (Supplementary Figure S3, S4). The Wetherill Concordia diagram and chondrite-normalized REE patterns for the analyzed zircons are displayed in Figure 8.

4.3.1 Vierručohkka banded amphibolite

Zircon is located in both melanocratic and leucocratic layers of the banded amphibolite (GUO1). They exhibit core-rim textures, predominantly characterized by oscillatory zoning (Supplementary Figure S3). Forty-nine U-Pb analyses were performed on a total of thirty-two zircon grains. Fifteen results with <10% discordance were accepted from the analyses. Five U-Pb analyses of zircon cores yield a Concordia age of 626.3 ± 6.9 Ma (MSWD = 0.75; Figures 8A, B). Seven analyses of zircon rims define a Concordia age of 598.8 ± 2.8 Ma (MSWD = 1.2; Figures 8A, B). Two analyses from zircon rims gave a younger Concordia age of 469 ± 2.1 Ma (MSWD = 0.62). Forty-seven trace element analyses were obtained from the same thirty-two zircons; LREE were typically below the detection limits. Thirty-two Eu anomalies were calculated ($Eu/Eu^* = Eu_N/\sqrt{(Sm_N * Gd_N)}$) ranging from 0.24 to 0.57. The slope of HREE is steep with Lu_N/Gd_N values ranging from 10.99–49.18 (an extreme value is excluded from the calculation; Figure 8C). The Th/U ratios range from 0.33–0.83.

4.3.2 Aurek Assemblage

Zircon from the Aurek gabbro (ARK13) predominantly display sector zoning (Supplementary Figure S4). A total of thirteen U-Pb analyses were performed on eleven zircon grains. All results were accepted as they were <10% discordant. One U-Pb analysis yielded a Concordia age of 670.2 ± 7.7 Ma (MSWD = 0.56; Figure 8D). Nine core measurements indicate a Concordia age of 614.4 ± 2.0 Ma (MSWD = 0.36; Figures 8D, E). Two rim analyses yielded a Concordia age of 600.6 ± 4.3 Ma (MSWD = 2.1; Figure 8D). Nine trace element analyses were obtained from nine zircon cores. Five Eu anomalies were calculated to range from 0.11–0.70. The slope of HREE is steep with Lu_N/Gd_N values ranging from 3.49–25.28 (Figure 8F). The Th/U ratios range from 0.05–0.64. Zircon from the Aurek amphibolite (ARK11) shows

TABLE 2 Representative EPMA data of the Aurek metagabbro (ARK6; ARK8). Formulae based on 12 oxygens (garnet), 24 oxygens (amphibole), 6 oxygens (pyroxene), 11 oxygens (micas) and 8 oxygens (plagioclase). Oxides are expressed in wt%, cations in a.p.f.u.

ARK6	Opx	Opx	Pl	Amph	Grt rim	Grt core	ARK8	Cpx	Pl	Amph	Grt rim	Grt core
SiO_2	55.92	55.06	50.10	48.80	38.75	38.98	SiO_2	53.01	59.96	49.15	37.87	37.76
TiO_2	0.00	0.02	0.00	0.07	0.00	0.03	TiO_2	0.02	0.00	0.68	0.01	0.11
Al_2O_3	0.36	0.71	32.77	10.84	21.99	22.23	Al_2O_3	1.98	25.09	7.66	21.69	21.33
Cr_2O_3	0.02	0.00	1.05	0.04	0.00	0.03	Cr_2O_3	0.09	0.13	0.05	0.06	0.24
FeO	15.18	15.35	0.16	0.03	21.55	20.67	FeO	19.06	0.00	13.7	26.14	27.46
MnO	0.11	0.07	0.00	6.49	0.59	0.69	MnO	0.10	0.00	0.11	0.81	1.56
MgO	28.62	28.14	0.11	17.47	6.34	5.80	MgO	11.82	0.01	13.44	4.01	3.85
CaO	0.33	0.23	8.10	11.92	11.27	11.79	CaO	12.64	7.12	11.65	9.74	8.11
K_2O	0.00	0.00	0.26	1.50	0.00	0.03	K_2O	0.19	0.07	0.35	0.02	0.03
Na_2O	0.00	0.00	6.71	0.21	0.02	0.01	Na_2O	0.22	7.34	1.36	0.01	0.07
Total	100.54	99.59	99.26	97.38	100.51	100.25	Total	99.13	99.72	98.15	100.37	100.52
Si	1.991	1.980	2.263	6.895	2.972	2.987	Si	2.023	2.663	7.131	2.966	2.967
Ti	0.000	0.001	0.000	0.008	0.000	0.002	Ti	0.001	0.000	0.074	0.001	0.007
Al	0.015	0.030	1.737	1.605	1.988	2.007	Al	0.089	1.313	1.309	2.002	1.975
Cr	0.001	0.000	0.037	0.005	0.000	0.002	Cr	0.003	0.004	0.006	0.004	0.015
Fe^{2+}	0.452	0.462	0.006	0.872	1.382	1.324	Fe^{2+}	0.609	0.000	1.662	1.712	1.804
Mn	0.003	0.002	0.000	0.006	0.038	0.045	Mn	0.003	0.000	0.014	0.054	0.104
Mg	1.519	1.509	0.007	3.680	0.725	0.663	Mg	0.673	0.001	2.907	0.468	0.451
Ca	0.013	0.009	0.390	1.805	0.926	0.968	Ca	0.517	0.339	1.811	0.817	0.683
K	0.000	0.000	0.015	0.038	0.000	0.002	K	0.009	0.004	0.065	0.002	0.003
Na	0.000	0.000	0.498	0.411	0.003	0.001	Na	0.016	0.632	0.382	0.002	0.010
Total	3.995	3.993	4.954	15.325	8.034	8.001	Total	3.943	4.957	15.361	8.027	8.018
^{X}Fe	0.229	0.234		0.192	0.656	0.667	^{X}Fe	0.475		0.364	0.785	0.800
^{X}En	0.765	0.761					^{X}En	0.373				
^{X}Wo	0.006	0.004					^{X}Wo	0.287				
^{X}Fs	0.229	0.234					^{X}Fs	0.340				
^{X}Ac	0.000	0.000					^{X}Ac	0.009				
^{X}Ab			0.385				^{X}Ab		0.481			
^{X}An			0.604				^{X}An		0.516			
^{X}Or			0.016				^{X}Or		0.004			
^{X}Alm					0.450	0.442	^{X}Alm				0.561	0.593

(Continued on the following page)

TABLE 2 (*Continued*) Representative EPMA data of the Aurek metagabbro (ARK6; ARK8). Formulae based on 12 oxygens (garnet), 24 oxygens (amphibole), 6 oxygens (pyroxene), 11 oxygens (micas) and 8 oxygens (plagioclase). Oxides are expressed in wt%, cations in a.p.f.u.

ARK6	Opx	Opx	Pl	Amph	Grt rim	Grt core	ARK8	Cpx	Pl	Amph	Grt rim	Grt core
^{X}Prp					0.236	0.221	^{X}Prp				0.153	0.148
^{X}Grs					0.302	0.323	^{X}Grs				0.268	0.224
^{X}Sps					0.012	0.015	^{X}Sps				0.018	0.034

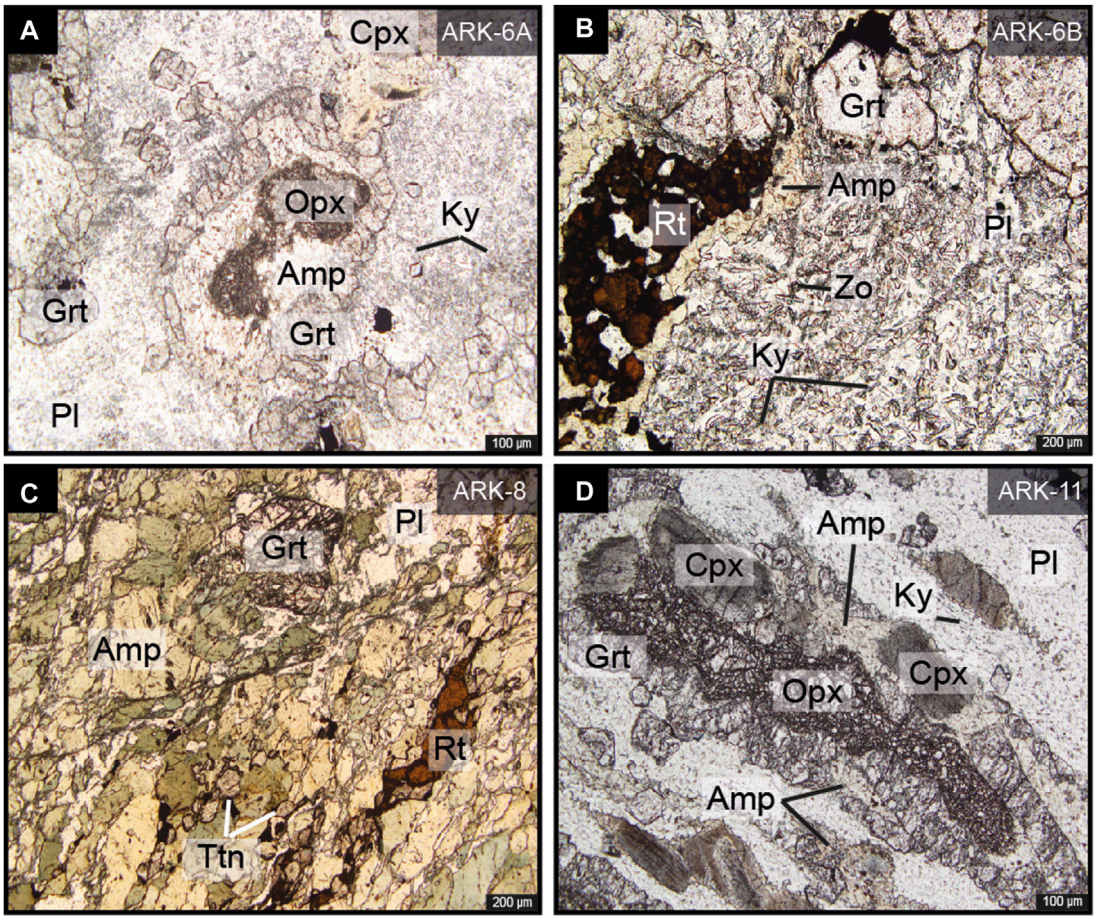

FIGURE 4
Photomicrographs of the Aurek metagabbro **(A, B)** and the Aurek amphibolite **(C, D)**. **(A)** orthopyroxene + amphibole surrounded by coronitic garnet. Kyanite lamellae replacing plagioclase. **(B)** Kyanite and zoisite lamellae replacing plagioclase and rutile crystals. **(C)** Representative photomicrograph of the Aurek amphibolite: amphibole + garnet + plagioclase + titanite + rutile. **(D)** Coronitic garnet surrounding clinopyroxene and orthopyroxene grain. Kyanite lamellae replacing plagioclase. All photomicrographs taken in plane polarized light.

core-rim textures (Supplementary Figure S4). A total of forty-eight U-Pb analyses were performed on twenty-two zircon grains. Thirty-eight results showed <10% discordance and were accepted for further statistical treatment. Thirty-five U-Pb cores analyses yield Concordia age of 609.3 ± 1.6 Ma (MSWD = 0.92; Figures 8G, H). Results from two rim measurements indicate a Concordia age of 523.1 ± 7.4 Ma (MSWD = 0.15; Figure 8G). Two more rim analyses defined a Concordia age of 424.9 ± 8.5 Ma (MSWD = 0.09; Figure 8G). Thirteen trace elements analyses were obtained from thirteen zircon grains. Seven Eu anomalies were calculated from 0.09 to 0.36. The slope of HREE is steep with LuN/GdN values ranging from 15.60 to 38.15 (Figure 8I). The Th/U ratios range from 0.28 to 0.62.

5 Discussion

5.1 Protolith crystallization age

Efforts to determine the timing of emplacement of the Baltoscandian dyke swarm related to Neoproterozoic rifting have

10.3389/feart.2024.1426525

TABLE 3 Representative EPMA data of the Aurek amphibolite (ARK14; ARK11). Formulae based on 12 oxygens (garnet), 24 oxygens (amphibole), 6 oxygens (pyroxene), 11 oxygens (micas) and 8 oxygens (plagioclase). Oxides are expressed in wt%, cations in a.p.f.u.

ARK14	Cpx	Cpx	Pl	Amph	Grt rim	Grt core	ARK11	Cpx	Opx	Pl	Amph	Grt rim	Grt core
SiO_2	53.82	53.96	55.66	52.26	39.08	38.55	SiO_2	53.82	54.60	52.83	41.80	34.27	38.70
TiO_2	0.33	0.22	0.03	0.35	0.01	0.00	TiO_2	0.76	0.94	0.00	0.91	0.00	0.06
Al_2O_3	2.05	1.87	28.39	6.16	22.25	22.12	Al_2O_3	2.57	0.95	30.38	16.97	19.18	21.21
Cr_2O_3	0.72	0.59	0.02	0.76	0.42	1.74	Cr_2O_3	0.38	0.07	0.06	0.31	13.46	1.90
FeO	4.06	4.07	0.12	7.41	22.19	21.23	FeO	4.73	18.17	0.00	11.08	17.41	25.83
MnO	0.10	0.06	0.03	0.05	0.62	0.67	MnO	0.06	0.28	0.01	0.01	0.52	0.82
MgO	14.62	14.86	0.03	17.48	7.62	7.19	MgO	15.23	24.49	0.01	11.27	5.95	5.11
CaO	23.55	23.56	10.38	12.72	8.04	8.94	CaO	22.25	1.98	12.94	11.84	8.26	6.90
K_2O	0.00	0.04	0.01	0.09	0.03	0.01	K_2O	0.58	0.02	0.05	1.060	0.04	0.00
Na_2O	0.80	0.65	5.33	0.66	0.02	0.10	Na_2O	0.03	0.04	3.86	2.25	0.11	0.08
Total	100.04	99.87	100.01	97.95	100.27	100.55	Total	100.41	101.54	100.15	97.51	99.20	100.61
Si	1.970	1.977	2.493	7.553	2.985	2.946	Si	1.960	1.968	2.375	6.125	2.718	3.003
Ti	0.009	0.006	0.001	0.037	0.000	0.000	Ti	0.021	0.026	0.000	0.101	0.000	0.003
Al	0.088	0.081	1.493	0.647	2.003	1.992	Al	0.110	0.040	1.609	2.931	1.793	1.939
Cr	0.021	0.017	0.001	0.085	0.026	0.105	Cr	0.011	0.002	0.002	0.036	0.844	0.117
Fe^{2+}	0.124	0.125	0.005	0.872	1.417	1.357	Fe^{2+}	0.144	0.548	0.000	1.358	1.155	1.676
Mn	0.003	0.002	0.001	0.006	0.040	0.043	Mn	0.002	0.009	0.000	0.002	0.035	0.054
Mg	0.798	0.812	0.002	3.666	0.868	0.819	Mg	0.827	1.316	0.001	2.462	0.703	0.591
Ca	0.924	0.925	0.496	1.918	0.658	0.732	Ca	0.868	0.076	0.623	1.859	0.702	0.574
K	0.000	0.002	0.001	0.017	0.003	0.000	K	0.027	0.002	0.003	0.198	0.004	0.000
Na	0.057	0.046	0.470	0.181	0.002	0.015	Na	0.001	0.002	0.336	0.640	0.017	0.012
Total	3.994	3.992	4.962	14.982	8.002	8.010	Total	3.972	3.989	4.950	15.712	7.970	7.969
^{X}Fe	0.135	0.133		0.192	0.620		^{X}Fe	0.148	0.294		0.355	0.621	0.739
^{X}En	0.432	0.436					^{X}En	0.449	0.675				
^{X}Wo	0.500	0.496					^{X}Wo	0.472	0.039				
^{X}Fs	0.069	0.068					^{X}Fs	0.079	0.285				
^{X}Ac	0.030	0.024					^{X}Ac	0.001	0.001				
^{X}Ab			0.317				^{X}Ab			0.212			
^{X}An			0.682				^{X}An			0.786			
^{X}Or			0.001				^{X}Or			0.003			

(Continued on the following page)

TABLE 3 (*Continued*) Representative EMPA data of the Aurek amphibolite (ARK14; ARK11). Formulae based on 12 oxygens (garnet), 24 oxygens (amphibole), 6 oxygens (pyroxene), 11 oxygens (micas) and 8 oxygens (plagioclase). Oxides are expressed in wt%, cations in a.p.f.u.

ARK14	Cpx	Cpx	Pl	Amph	Grt rim	Grt core	ARK11	Cpx	Opx	Pl	Amph	Grt rim	Grt core
^{X}Alm					0.475	0.460	^{X}Alm					0.445	0.579
^{X}Prp					0.291	0.278	^{X}Prp					0.271	0.204
^{X}Grs					0.221	0.248	^{X}Grs					0.271	0.198
^{X}Sps					0.013	0.015	^{X}Sps					0.013	0.019

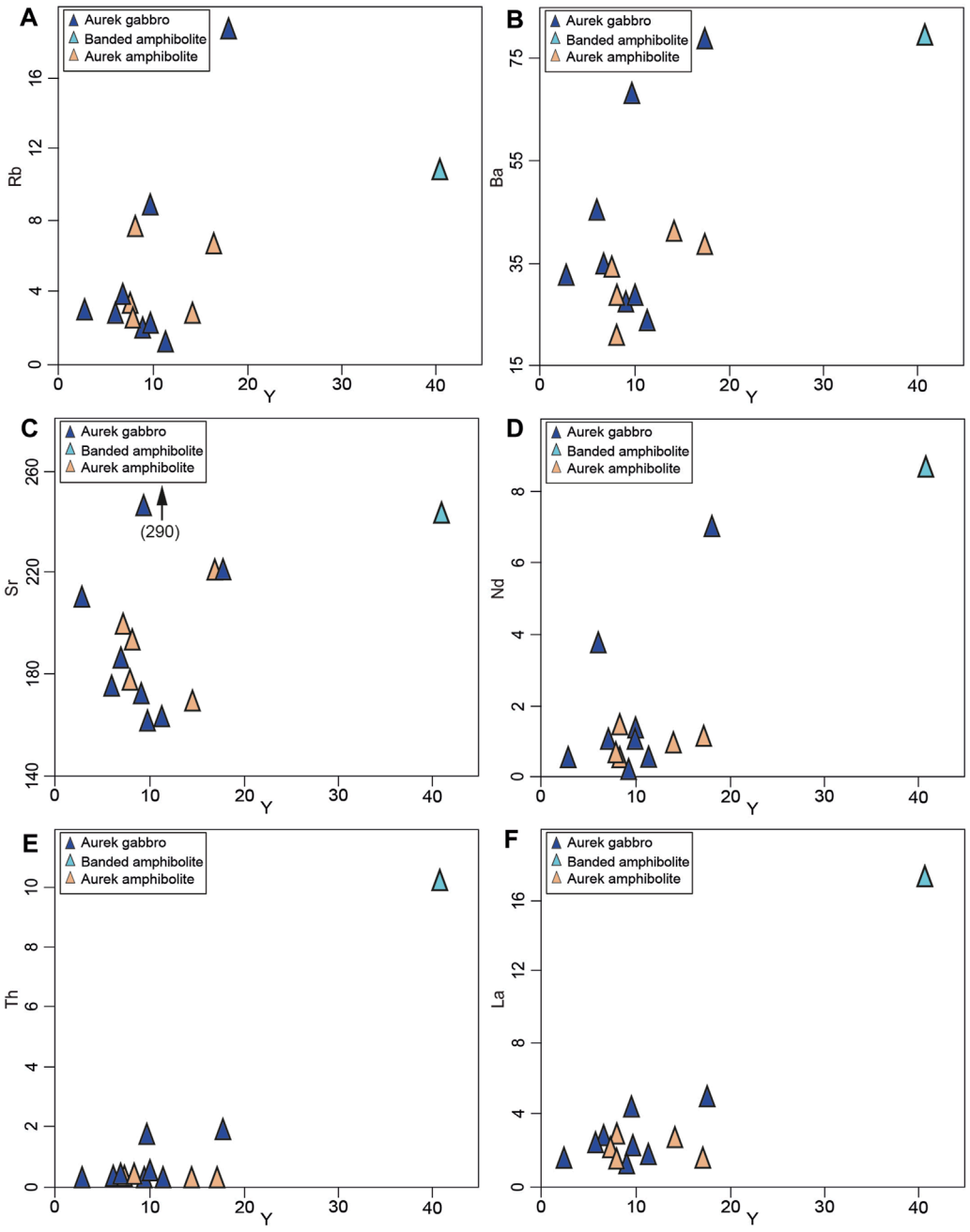

FIGURE 5
Trace element geochemistry for the banded amphibolite, Aurek gabbro and Aurek amphibolite. **(A)** Rb, **(B)** Ba, **(C)** Sr, **(D)** Nd, **(E)** Th, **(F)** La are plotted versus Y. Units are part per million (ppm).

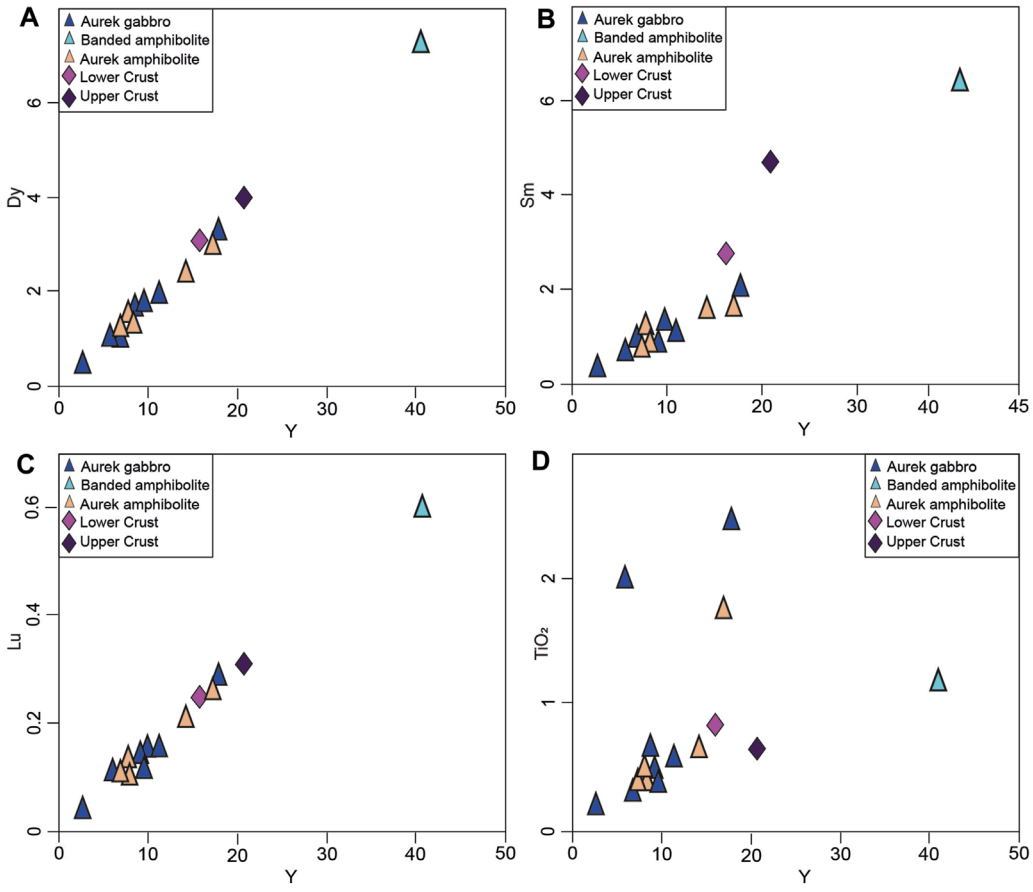

FIGURE 6
Trace element geochemistry tracing the metamorphic signature of the banded amphibolite, Aurek gabbro and Aurek amphibolite. **(A)** Dy, **(B)** Sm, **(C)** Lu, and **(D)** TiO_2 are plotted versus Y.

yielded a range of ages in different sections of the northern Caledonides. For example, the Sarek Dyke Swarm yielded a $^{207}Pb/^{206}Pb$ age of 608 ± 1 Ma (Svenningsen, 2001), while in the Kebnekaise region the U-Pb zircon ages range between 608 and 596 Ma (e.g., Paulson and Andréasson, 2002; Root and Corfu, 2012; Baird et al., 2014). Farther north in the Corrovarre Nappe, the dyke ages yielded 610 ± 1 Ma (Gee et al., 2016). In all the studied samples presented in this work, zircon grains have primitive magmatic REE patterns with steep HREE trends (Hoskin and Schaltegger, 2003). Based on the analysis of the internal oscillatory-zoned regions of the zircons and the zircon REE trends (Corfu et al., 2003; Rubatto, 2017), the oldest cluster of ages reported in this study are interpreted as the protolith crystallization ages. Cores of zircon in the banded amphibolite (GUO1) yielded the oldest age of 626 ± 7 Ma. The Aurek Gabbro (ARK-13) and the Aurek amphibolite (ARK-11) provided ages of 614 ± 2 Ma and 609 ± 2 Ma, respectively. Ages obtained in this study display a longer emplacement history of mafic magmatism than currently known from the Sarek Dyke complex and the Corrovarre Nappe. Furthermore, in the same Kebnekaise region, ages obtained by Baird et al. (2014) are younger than those obtained in this study, indicating prolonged mafic magmatism that started already at c. 626 Ma. Moreover, a younger age of 599 ± 3 Ma is also recorded by zircon rims in the banded amphibolite. This age, based on the texture of the zircons (Rubatto, 2017; Supplementary Figure S3) and the presence of partial melting features in the sample (Figures 3G, H), is interpreted as the age of the partial melting event. This age suggests that after the crystallization of the protolith of the banded amphibolite at c. 626 Ma, the Vierručohkka amphibolite partially remelted at c. 599 Ma probably due to the emplacement of a large volume of mafic magma. A comparable age of c. 600 Ma was obtained by Walczak et al. (2022) in the Váivančohkka region, northern Scandinavian Caledonides (Figure 1) applying U-Pb zircon and Th-U-total Pb monazite geochronology. They interpreted this age as the high-temperature anomaly related to the rifting process. Hence, our new data supports the hypothesis that the emplacement of the Aurek Assemblage could represent the cause of the same c. 600 Ma thermal anomaly inducing partial melting of the already crystallized protolith to form the banded amphibolite.

5.2 The metamorphic signature

In order to understand and recover the magmatic source signature of the studied samples, all other influences such as the

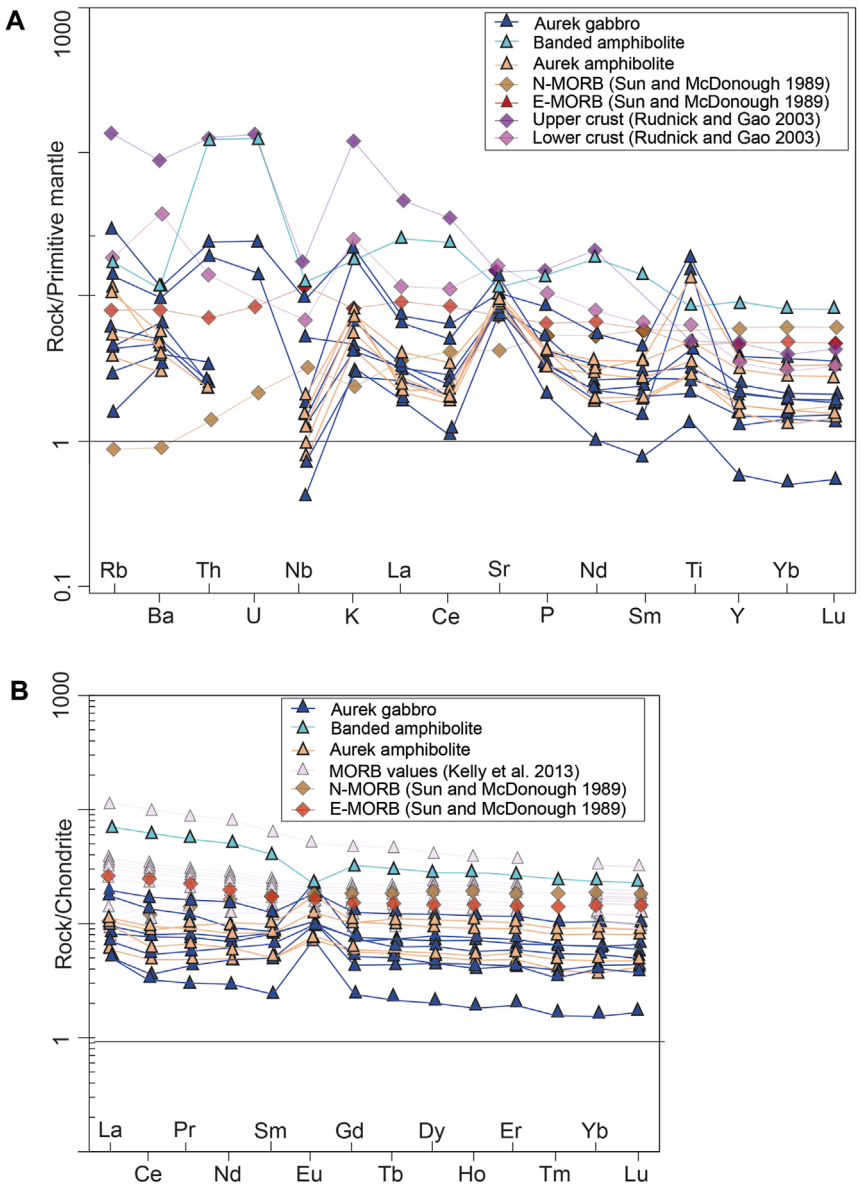

FIGURE 7
Spider diagram normalized to the primitive mantle and chondrite values of Sun and McDonough (1989). **(A)** Multi-elements diagram of the studied samples; **(B)** chondrite-normalized REE diagram of the studied rocks. For comparison average upper and lower crust values (Rudnick and Gao, 2003), MORB values (Kelley et al., 2013), and N-MORB and E-MORB (Sun and McDonough, 1989).

metamorphic contribution and the crustal assimilation need to be discussed and the corresponding geochemical signatures omitted from further discussion.

All the studied samples showed petrographic evidence of high-grade metamorphism. Specifically, the garnet of the banded amphibolite, which based on its textural position, shape, and zonation of the grossular component, is interpreted as peritectic garnet. Together with the melt pseudomorphs, and symplectite at the boundary of the amphibole grains, the garnet records that metamorphism in the melt stability field occurred at c. 599 Ma (Figures 3C, D, F–H; Supplementary Figure S2). Regarding the Aurek Assemblage rocks, the high-pressure metamorphism is apparent from the presence of coronitic garnet, and from the exsolution of kyanite and zoisite at the expense of plagioclase and amphibole (Figures 4A, B, D; e.g., Wayte et al., 1989; Schorn and Diener, 2017). This high-pressure event is interpreted as the progressive subduction during the Caledonian orogeny (e.g., Gee et al., 2013; Klonowska et al., 2017). Consequently, evidence of this metamorphism is visible in variations of the mineral texture and assemblages, and in the bulk rock geochemical signatures of the investigated samples.

The high-grade metamorphic signature affects the whole-rock compositions, in particular, the Dy, Sm, Lu, and Y contents record the growth of metamorphic/peritectic garnet, with the highest value recorded by the banded amphibolite (Figures 6A–C). The high-pressure metamorphism is also traced in the Aurek gabbro by elevated TiO_2 attributed to the crystallization of metamorphic rutile (Figure 6D). LILE are commonly mobilized

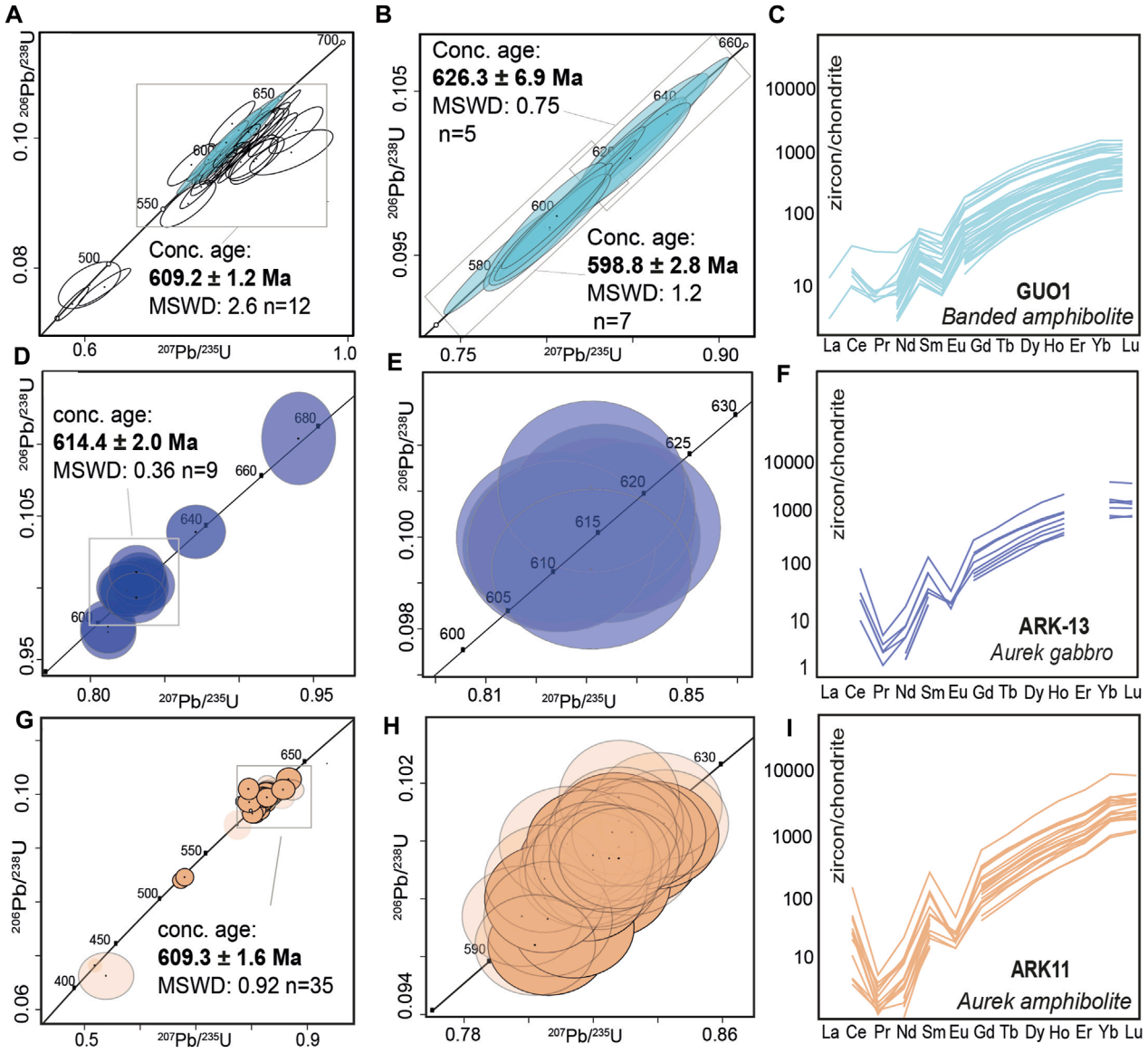

FIGURE 8
Analytical results for U–Pb zircon geochronology. **(A)** Wetherill concordia diagram for zircons of GUO1. Blue ellipses correspond to concordant analysis. **(B)** Magnification of the grey box in **(A)** representing concordant analyses of zircon cores and rims. **(C)** Chondrite-normalized REE patterns for sample GUO1. **(D)** Wetherill concordia diagram for zircons of ARK-13. **(E)** Magnification of the grey box in **(D)** representing concordant analyses of zircon rims. **(F)** Chondrite-normalized REE patterns for sample ARK13. **(G)** Wetherill concordia diagram for zircons of ARK-11. **(H)** Magnification of the grey box in **(G)** representing concordant analyses of zircon rims. **(I)** Chondrite-normalized REE patterns for sample ARK-11.

in fluids associated with metamorphism (e.g., Ridley, 2012), and for this reason Rb and Ba are expected to be depleted during high-pressure metamorphism due to metamorphic dehydration reactions (e.g., Zack and John, 2007). However, Rb and Ba are not depleted as expected, plotting within the range of MORB values (Figures 9A, B). Furthermore, Sr shows scattered enrichment relative to MORB values (Figure 9C). This is interpreted as a result of crustal assimilation rather than extensive fluid-rock interaction between the protolith and the surrounding sediments, since the latter should lead to a relative loss of Sr (e.g., Barker et al., 2008; Gołuchowska et al., 2022). However, a later fluid-rock interaction cannot be ruled out. Generally, the metamorphic overprint is best traced by elements such as Dy, Lu, Sm, Y and also TiO_2 contents, and consequently, these elements cannot be used in the further interpretation of the magmatic source signature of the studied samples.

5.3 Crustal assimilation of the banded amphibolite and Aurek assemblage magmas

The banded Vierručohkka amphibolite and the Aurek Assemblage were located at the outermost Baltica margin prior to the rifting event (Gee et al., 2020). Therefore, magmas must have been transported through the continental crust in order to

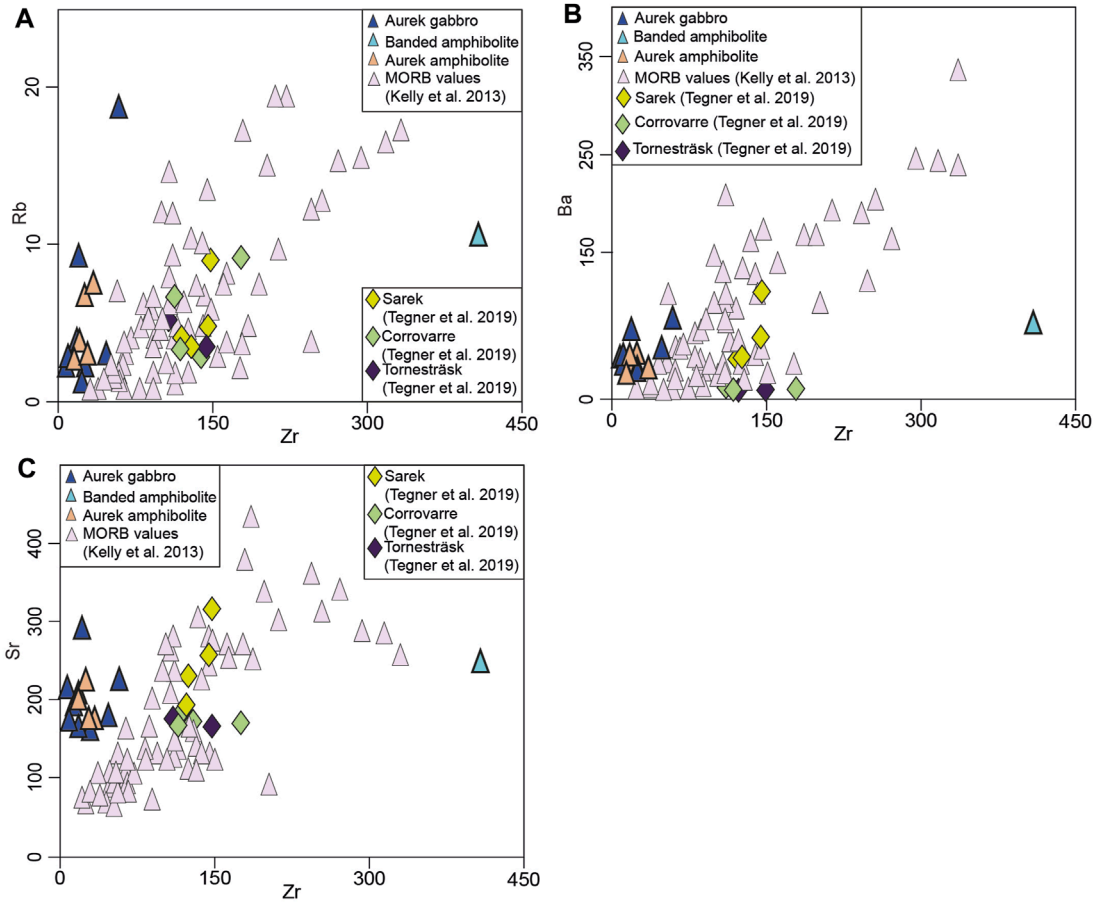

FIGURE 9
LILE geochemistry of the Aurek gabbro and Aurek amphibolite. All the units are in ppm. **(A)** Rb, **(B)** Ba, **(C)** Sr are plotted versus Zr. For comparison MORB (Kelley et al., 2013), Sarek, Corrovarre, and Torneträsk metavolcanic samples (without crustal assimilation signature; Tegner et al., 2019).

be emplaced into metasedimentary upper crustal rocks of the Leavasvággi gneiss (Callegari et al., 2023). For this reason, the influence of magma-crust interaction on the geochemistry of the studied samples is considered. The Aurek metagabbro and amphibolite, and the banded amphibolite display elevated Th/Nb and La/Nb content (Figure 10A). The feature is visible also in Th/Yb and Nb/Yb ratios (Figures 10A, B). Here, all the samples are enriched toward lower and upper crust compositions (Figure 10B). The samples from this study are compared with Baltoscandian dyke swarm samples from the Sarek, Corrovarre and Torneträsk regions, which yield crystallization ages of c. 600 Ma, and are characterized by crustal assimilation (Tegner et al., 2019). Data obtained by Tegner et al. (2019) display comparable values of Th/Nb and La/Nb to the Aurek samples and the banded amphibolite (Figure 10A). Moreover, the similarity is also visible for the Th/Yb and Nb/Yb ratios and all the samples show an affinity to lower crust assimilation (Figures 10A–C). The banded amphibolite and a sample from Torneträsk suggest upper crust assimilation (elevated Th/Nb and La/Nb; Figure 10A), however, we cannot exclude the concurrency of both lower and upper crust assimilation (Figures 10A, C).

It is widely accepted that the Appalachians record the rifting of Laurentia following the break-up of Rodinia and opening of the Iapetus Ocean (e.g., Cawood and Nemchin, 2001). For this reason, the Neoproterozoic dykes outcropping in the Appalachians are considered a Laurentian counterpart to the Neoproterozoic dyke swarm exposed in the Caledonides (e.g., Williams and Hiscott, 1987). In this work, we compared the new geochemical data presented here with a compilation of Neoproterozoic tholeiitic magmatic rocks from a depleted mantle source associated with a large igneous province exposed in the Appalachians (Bédard and Stevenson, 1995; Camiré et al., 1995; Cawood and Nemchin, 2001; Dennis et al., 2004). Additionally, we compare our data with a compilation of volcanic rocks from the Cenozoic depleted magmatism due to crustal hyperextension not related with a large igneous province/mantle plume (Basin and Range mafic rocks; e.g., Wang et al., 2002; compilation from: Dungan et al., 1986). The Th/Yb, Nb/Yb, and Th/La contents are very similar throughout all the samples (Figures 10A–C). Nevertheless, Caledonide samples display lower crustal affinity (Figure 10A) while the Appalachians and the Basin and Range samples display higher contributions of upper crustal assimilation (Figures 10B, C). Different degrees of crustal assimilation suggested by the Th/Nb and Th/Yb (Figures 10A,B) are visible not only between the Laurentia and Baltica samples, but within the same suite of dykes from the Caledonides. This suggests that the amount of crustal assimilation and the type of assimilated crust are locally controlled by the

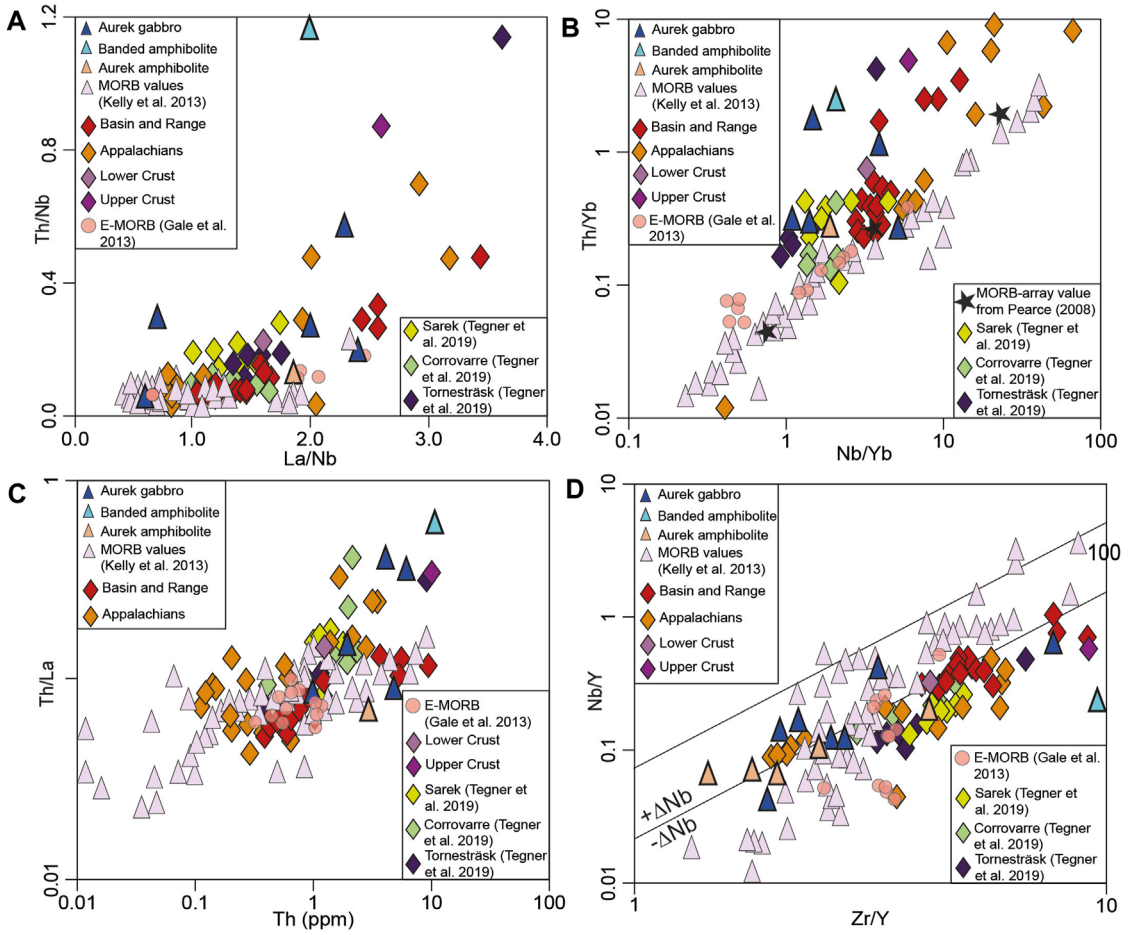

FIGURE 10
Trace element ratios for the banded amphibolite, Aurek gabbro and Aurek amphibolite. **(A)** La/Nb vs. Th/Nb, **(B)** Nb/Yb vs. Th/Yb, **(C)** Th vs. Th/La, **(D)** Zr/Y vs. Nb/Y. For comparison MORB (Kelley et al., 2013), E-MORB (Gale et al., 2013), MORB-array value (Pearce, 2008), Sarek, Corrovarre, and Torneträsk metavolcanic samples (with crustal assimilation signature; Tegner et al., 2019), Appalachia Neoproterozoic volcanic rocks (Bédard and Stevenson, 1995; Camiré et al., 1995; Dennis et al., 2004), and Basin and Range volcanic rocks (Dungan et al., 1986). ΔNb = 1.74 + log(Nb/Y) - 1.92 log(Zr/Y) after Fitton et al. (1997).

surrounding country rocks. Only speculation on the type of assimilated crust is possible with the data presented in this work. The high values in Th, La, Th/Yb, and Nb/Yb suggest the assimilation of felsic and mafic rocks belonging to the nearby Vássačorru Igneous Complex. This bimodal igneous suite is characterized by a composition with lower crust affinity and crystallization ages between c. 865 Ma to c. 830 Ma (e.g., Jakob et al., 2022; Callegari et al., 2023). Other lithologies for assimilants could include upper crustal quartz-feldspathic gneiss, calc-silicate gneiss, and bodies of meta-dolerite all of which belong to the Leavasvággi Gneiss (e.g., Andréasson et al., 2018).

5.4 Continental rifting and source recorded by the banded amphibolite and Aurek Assemblage

Having determined the signature of the metamorphism and the crustal assimilation in the geochemical dataset, the Th, U, La, Nd, Nb, and Zr contents as well as ratios are used to determine the source of the magmas and the origin of the continental magmatism between c. 625 Ma and c. 610 Ma. From the presented dataset, samples with Th/Nb values higher than 0.15 have not been considered in order to exclude samples affected by crustal assimilation. The same approach is used for the samples from Sarek, Corrovarre and Torneträsk by Tegner et al. (2019). The HFSE (Th, U, Zr, Nb, La, Nd) show trends of fractional crystallization, which is evidence that they can be used to trace the magmatic source since the ratios of these elements are not affected by metamorphism or crustal assimilation (Figures 11A–C). The studied samples do not show any differences in the composition of Th, U, La, Nd, and Zr between Aurek metagabbro and amphibolite suggesting a common magmatic source for the protoliths of these two sample suites (Figure 11). Generally, Th, U, and Nd versus Zr plot toward low concentrations with respect to the more enriched dyke samples from Sarek, Corrovarre, and Torneträsk presented by Tegner et al. (2019) (Figures 11A–C). The trace element geochemistry of the Aurek gabbro and Aurek amphibolite correspond to a MORB

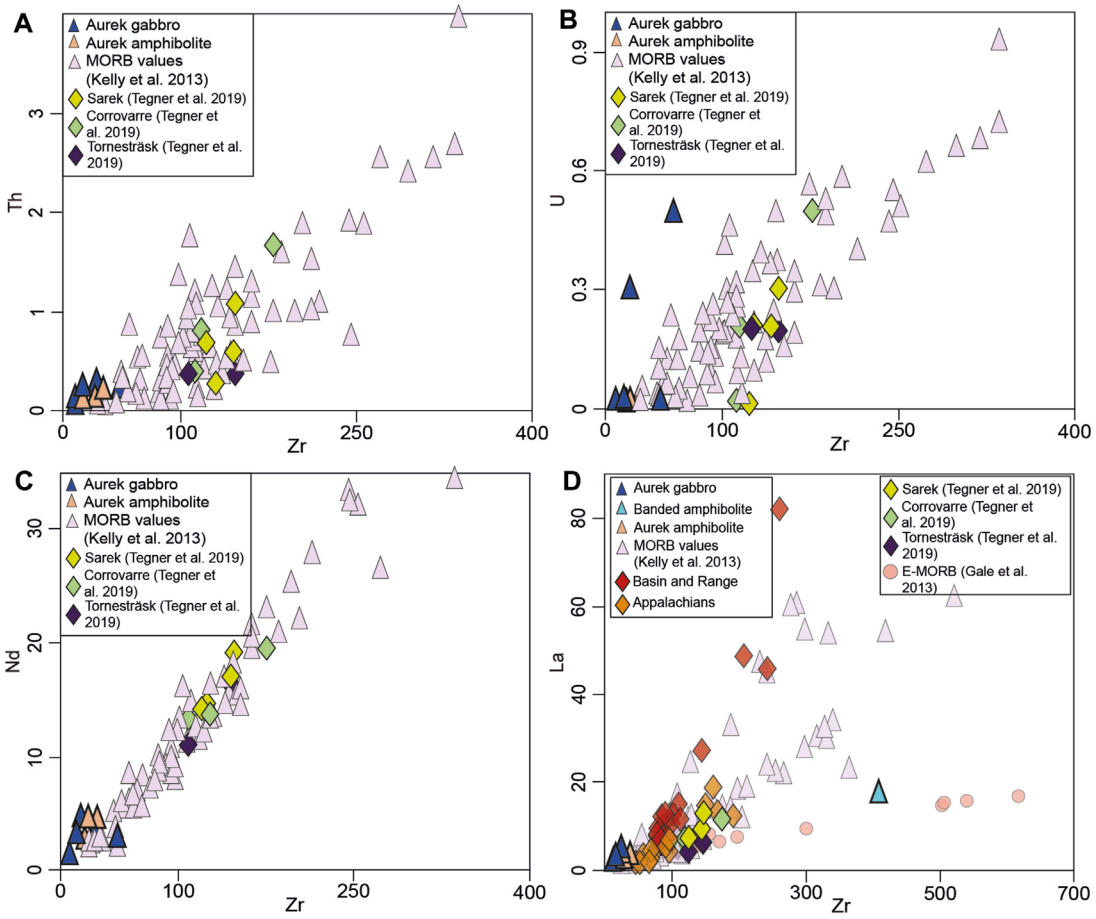

FIGURE 11
HFSE geochemistry indicating the source signature of the Aurek gabbro and Aurek amphibolite. All the units are in ppm. **(A)** Th, **(B)** U, **(C)** Nd, and **(D)** La are plotted versus Zr. For comparison MORB (Kelley et al., 2013), E-MORB (Gale et al., 2013), Sarek, Corrovarre, and Torneträsk metavolcanic samples (without crustal assimilation signature; Tegner et al., 2019).

affinity (Figures 10A–C). The samples often display near MORB values and extend to higher Th/Nb, La/Nb, Th/Yb, and Nb/Yb reaching more precisely the field of E-MORB (Figures 10A, B). These observations are confirmed by ΔNb (Fitton et al., 1997), where most of the samples display negative values similar to both N-MORB and E-MORB (Figure 10D). The same observations are found for the Appalachian samples (Figures 10A–D). However, the Sarek, Corrovarre, and Torneträsk samples display relatively elevated Nd and Zr values with respect to the studied samples (Figure 11C). Moreover, the La and Zr concentrations show evidence of an enriched mantle source (i.e., mantle plume; Figure 11D; Tegner et al., 2019). The studied samples, altogether with the sample suites from the Appalachians, display lower values of La and Zr with respect to the Sarek, Corrovarre and Torneträsk dykes (Tegner et al., 2019), suggesting a similar upper mantle source for their magmas (Figure 11D). Nevertheless, the formation of the Baltoscandian dyke swarm is related to a mantle plume which is providing the enriched source for the geochemistry signature of the samples from Sarek, Corrovarre and Torneträsk (Figure 1; Tegner et al., 2019). Contemporaneously, the studied samples from the Aurek Assemblage indicate a depleted upper mantle source (Figures 6, 11) similar to the Appalachian samples. These observations are not contradictory, rather they suggest a possible heterogeneity in the mantle sources (e.g., Hastie et al., 2016). From a continental rifting process, we speculate about the potential location of the mantle-plume and the relative position of the different samples with respect to the mantle-plume. The samples studied by Tegner et al. (2019) are characterized by an E-MORB signature and interpreted as mantle-plume related suggesting a geographical proximity to the mantle-plume itself. The samples studied in this work instead, filtered for possible influences of metamorphism and crustal assimilation on the geochemistry, have a depleted upper mantle signature. Specifically, this may suggest that the protolith of the Aurek Assemblage samples represents crustal thinning that induced mantle melting distal from the mantle-plume, which sampled the depleted upper mantle (N-MORB). In this scenario, the suggested mantle-plume should be located farther north than the Corrovarre region (Figure 1; present-day coordinates) however more work needs to be conducted to address this question.

Altogether, the REE pattern (Figure 6), trace element geochemistry, and the ΔNb values suggest magmatism tapping

into a depleted mantle source beneath the continental crust which indicates continental rift as the mechanism for the formation of the banded amphibolite and Aurek Assemblage magmas.

6 Conclusion

The Neoproterozoic continental rifting recorded in the Seve Nappe Complex in the northern Scandinavian Caledonides is revealed by new U-Pb zircon geochronology to commence at c. 625 Ma, which is recorded by the Vierručohkka amphibolite, and by the c. 614 Ma and c. 609 Ma crystallization of the Aurek gabbro and Aurek amphibolite, respectively. A partial melting event at c. 599 Ma is also recorded in the banded amphibolite. This confirms the southerly extension of the c. 600 Ma partial melting event already recognized in the Váivančohkka-Salmmečohkat region. Evidence of upper crust and lower crust assimilation are recorded in the banded amphibolite and the Aurek Assemblage, respectively. Similar geochemical signatures are recorded in the samples from the Appalachians, suggesting a similar assimilation and source history. The HFSE together with ΔNb indicate a depleted mantle source for the Vierručohkka amphibolite and the Aurek Assemblage magmas, similar to the Appalachian dykes. Values of Dy, Sm, Lu, and Y are used to trace the crystallization of metamorphic garnet. Enriched TiO_2 content implies the crystallization of metamorphic rutile. The geochemical variations of Dy, Sm, Lu, Y and TiO_2 indicate prograde metamorphism probably occurring in the subducting slab during the Caledonian orogeny. U-Pb zircon geochronology coupled with geochemical analysis indicate that the magmatism responsible for igneous lithologies present in the Kebnekaise region is related to the mantle-plume driven continental rifting of Rodinia between c. 625 and c. 609 Ma, responsible for the emplacement of the Central Iapetus Magmatic Province.

Data availability statement

The original contributions presented in the study are included in the article/Supplementary Material, further inquiries can be directed to the corresponding author.

Author contributions

RC: Conceptualization, Data curation, Formal Analysis, Investigation, Software, Visualization, Writing–original draft. AB: Conceptualization, Data curation, Investigation, Supervision, Writing–review and editing. CB: Investigation, Supervision, Validation, Writing–review and editing. KW: Validation, Writing–review and editing. GZ: Validation, Writing–review and editing. IK: Validation, Writing–review and editing. EK: Formal Analysis, Methodology, Validation, Writing–review and editing. SR: Validation, Writing–review and editing. KK: Formal Analysis, Supervision, Validation, Writing–review and editing. JM: Conceptualization, Formal Analysis, Resources, Supervision, Validation, Writing–review and editing.

Funding

The author(s) declare that financial support was received for the research, authorship, and/or publication of this article. This work was funded by the National Science Centre (Poland), IAPETUS project no. 2019/33/B/ST10/01728 to JM.

Acknowledgments

The authors are grateful to Editor Zhaochong Zhang, Junhong Zhao, and Veronica Peverelli for their suggestions and comments, which guided the manuscript revisions. We acknowledge the Vetenskapsrådet-funded NordSIMS-Vegacenter infrastructure (Dnr. 2021-00276) for provisioning of facilities and we would like to thank M. Kielman-Schmitt for sample preparation and analytical assistance. This is Vegacenter publication #079.

Conflict of interest

The authors declare that the research was conducted in the absence of any commercial or financial relationships that could be construed as a potential conflict of interest.

The author(s) declared that they were an editorial board member of Frontiers, at the time of submission. This had no impact on the peer review process and the final decision.

Publisher's note

Supplementary material

The Supplementary Material for this article can be found online at: https://www.frontiersin.org/articles/10.3389/feart.2024.1426525/full#supplementary-material

References

Andersen, T. B., Corfu, F., Labrousse, L., and Osmundsen, P.-T. (2012). Evidence for hyperextension along the pre-Caledonian margin of Baltica. *J. Geol. Soc.* 169 (5), 601–612. doi:10.1144/0016-76492012-011

Andréasson, P. G. (1994). The Baltoscandian margin in Neoproterozoic-early palaeozoic times. Some constraints on terrane derivation and accretion in the Arctic Scandinavian Caledonides. *Tectonophysics* 231, 1–32. doi:10.1016/0040-1951(94)90118-x

Andréasson, P. G., and Albrecht, L. (1995). Derivation of 500 Ma eclogites from the passive margin of Baltica and a note on the tectonometamorphic heterogeneity of eclogite-bearing crust. *Geol. Mag.* 132, 729–738. doi:10.1017/s001675680001894x

Andréasson, P. G., Allen, A., Aurell, O., Boman, D., Ekestubbe, J., Goerke, U., et al. (2018). Seve terranes of the Kebnekaise Mts., Swedish Caledonides, and their amalgamation, accretion and affinity. *GFF* 136, 264–291. doi:10.1080/11035897.2018.1470200

Baird, G. B., Figg, S. A., and Chamberlain, K. R. (2014). Intrusive age and geochemistry of the Kebne dyke complex in the Seve nappe complex, Kebnekaise massif, arctic Sweden Caledonides. *GFF* 136, 556–570. doi:10.1080/11035897.2014.924553

Barker, A. K., Coogan, L. A., Gillis, K. M., and Weis, D. (2008). Strontium isotope constraints on fluid flow in the sheeted dike complex of fast spreading crust: pervasive fluid flow at Pito Deep. *Geochem. Geophys. Geosystem* 9, Q06010. doi:10.1029/2007GC001901

Barnes, C. J., Majka, J., Callegari, R., Walczak, K., Ziemniak, G., and Bukała, M. (2023). Ordovician–Silurian deformation of the Neoproterozoic upper gneiss unit in the northern Seve Nappe Complex: implications for subduction of the Baltican margin. *J. Geol. Soc.* 180. doi:10.1144/jgs2022-161

Barnes, C. J., Majka, J., Schneider, D., Walczak, K., Bukała, M., Kośmińska, K., et al. (2019). High-spatial resolution dating of monazite and zircon reveals the timing of subduction–exhumation of the Vaimok Lens in the Seve Nappe Complex (Scandinavian Caledonides). *Contrib. Mineral. Petrol.* 174, 5. doi:10.1007/s00410-018-1539-1

Bedard, J. H., and Stevenson, R. (1995). The Caldwell Group lavas of southern Quebec: MORB-like tholeiites associated with the opening of Iapetus Ocean. *Can. J. Earth Sci.* 36, 999–1019. doi:10.1139/cjes-36-6-999

Bingen, B., Demaiffe, D., and Breemen, O. V. (1998). The 616 Ma old Egersund basaltic dike swarm, sw Norway, and late neoproterozoic opening of the Iapetus Ocean. *J. Geol.* 106 (5), 565–574. doi:10.1086/516042

Black, L. P., Kamo, S. L., Allen, C. M., Davis, D. W., Aleinikoff, J. N., Valley, J. W., et al. (2004). Improved $^{206}Pb/^{238}U$ microprobe geochronology by the monitoring of a trace-element-related matrix effect; SHRIMP, ID–TIMS, ELA–ICP–MS and oxygen isotope documentation for a series of zircon standards. *Chem. Geol.* 205, 115–140. doi:10.1016/j.chemgeo.2004.01.003

Bukała, M., Klonowska, I., Barnes, C., Majka, J., Kosminska, K., Janak, M., et al. (2018). UHP metamorphism recorded by phengite eclogite from the Caledonides of northern Sweden: P–T path and tectonic implications. *J. Metamorph. Geol.* 36, 547–566. doi:10.1111/jmg.12306

Burke, K., and Dewey, J. F. (1973). Plume-generated triple junctions: key indicators in applying plate tectonics to old rocks. *J. Geol.* 81, 406–433. doi:10.1086/627882

Callegari, R., Kośmińska, K., Barnes, J. C., Klonowska, I., Barker, A. K., Rousku, S., et al. (2023). Early neoproterozoic magmatism and caledonian metamorphism recorded by the Mårma terrane, Seve nappe complex, northern Swedish Caledonides. *J. Geol. Soc. Lond.* 180. doi:10.1144/jgs2022-092

Camiré, G., La Flége, M. R., and Jenner, G. A. (1995). Geochemistry of pre-taconian mafic volcanism in the humber zone of the northern Appalachians, quebec, Canada. *Chem. Geol.* 119, 55–77. doi:10.1016/0009-2541(94)00104-g

Cawood, P. A., and Nemchin, A. A. (2001). Paleogeographic development of the east Laurentian margin: constraints from U-Pb dating of detrital zircons in the Newfoundland Appalachians. *GSA Bull.* 113, 1234–1246. doi:10.1130/0016-7606(2001)113<1234:pdotel>2.0.co;2

Chew, D. M., and Van Staal, C. R. (2014). The ocean–continent transition zones along the Appalachian–Caledonian Margin of Laurentia: examples of large-scale hyperextension during the opening of the Iapetus Ocean. *Geosci. Can.* 41, 165–185. doi:10.12789/geocanj.2014.41.040

Corfu, F., Andersen, T. B., and Gasser, D. (2014). "The Scandinavian Caledonides: main features, conceptual advances and critical questions," in *New perspectives on the Caledonides of Scandinavia and related areas*. Editors F. Corfu, D. Gasser, and D. M. Chew (Geological Society London Special Publications), 390.

Corfu, F., Hanchar, J. M., Hoskin, P. W. O., and Kinny, P. (2003). Atlas of zircon textures. *Rev. Mineral. Geochem.* 53, 469–500. doi:10.2113/0530469

Dennis, A. J., Shervais, J. W., Mauldin, J., Maher, H. D., and Wright, J. E. (2004). Petrology and geochemistry of neoproterozoic volcanic arc terranes beneath the atlantic coastal plain, savannah river site, South Carolina. *GSA Bull.* 116, 572–593. doi:10.1130/b25240.1

Dungan, M. A., Lindstrom, M. M., McMillan, N. J., Moorbath, S., Hoefs, J., and Haskin, L. A. (1986). Open system magmatic evolution of the Taos Plateau volcanic field, northern New Mexico: 1. The petrology and geochemistry of the Servilleta Basalt. *J. Geophys. Res.* 91, 5999–6028. doi:10.1029/jb091ib06p05999

Ernst, R. E., and Bell, K. (2010). Large igneous provinces (LIPs) and carbonatites. *Mineral. Petrol.* 98, 55–76. doi:10.1007/s00710-009-0074-1

Fassmer, K., Frotzheim, N., Janák, M., Strohmeyer, M., Bukala, M., Lagos, M., et al. (2021). Diachronous collision in the Seve nappe complex: evidence from Lu–Hf geochronology of eclogites (norrbotten, north Sweden). *J. Metamorph. Geol.* 39, 819–842. doi:10.1111/jmg.12591

Fitton, J. G., Saunders, A. D., Norry, M. J., Hardarson, B. S., and Taylor, R. N. (1997). Thermal and chemical structure of the Iceland plume. *Earth Planet. Sci. Lett.* 153, 197–208. doi:10.1016/s0012-821x(97)00170-2

Gale, A., Dalton, C. A., Langmuir, C. H., Su, Y., and Schilling, J. G. (2013). The mean composition of ocean ridge basalts. *Geochem. Geophys. Geosystems* 14, 489–518. doi:10.1029/2012GC004334

Gee, D. G. (1975). A tectonic model for the central part of the Scandinavian Caledonides. *Am. J. Sci.* 275-A, 468–515.

Gee, D. G., Andréasson, P. G., Li, Y., and Krill, A. (2016). Baltoscandian margin, Sveconorwegian crust lost by subduction during Caledonian collisional orogeny. *GFF* 139 (1), 36–51. doi:10.1080/11035897.2016.1200667

Gee, D. G., Fossen, H., Henriksen, N., and Higgins, A. K. (2008). From the early paleozoic platforms of Baltica and Laurentia to the Caledonide orogen of Scandinavia and Greenland. *Episodes* 31, 44–51. doi:10.18814/epiiugs/2008/v31i1/007

Gee, D. G., Janák, M., Majka, J., Robinson, P., and van Roermund, H. (2013). Subduction along and within the baltoscandian margin during closing of the Iapetus Ocean and Baltica– Laurentia collision. *Lithosphere* 5, 169–178. doi:10.1130/l220.1

Gee, D. G., Klonowska, I., Andréasson, P.-G., and Stephens, M. B. (2020). Chapter 21 Middle thrust sheets in the Caledonide orogen, Sweden: the outer margin of Baltica, the continent–ocean transition zone and late Cambrian–Ordovician subduction–accretion, in *Sweden: lithotectonic framework, tectonic evolution and mineral Resources*. Editors M. B. Stephens, and J. Bergman Weihed Geological Society London Memoirs, 50, 517–548. doi:10.1144/M50-2018-73

Gee, D. G., Kumpulainen, R., Roberts, D., Stephens, M. B., Thon, A., and Zachrisson, E. (1985). *Scandinavian Caledonides: tectonostratigraphical map*. Uppsala: Sveriges Geologiska Undersokning.

Gilio, M., Clos, F., and Roermund, H. L. M. (2015). The Friningen garnet peridotite (central Swedish Caledonides). A good example of the characteristic PTt path of a cold mantle wedge garnet peridotite. *Lithos* 230, 1–16. doi:10.1016/j.lithos.2015.05.003

Gołuchowska, K., Barker, A., Manecki, M., Majka, J., Kośmińska, K., Ellam, R. M., et al. (2022). The role of crustal contamination in magma evolution of Neoproterozoic metaigneous rocks from Southwest Svalbard. *Precambrian Res.* 370, 106521. doi:10.1016/j.precamres.2021.106521

Harland, W. B., and Gayer, R. A. (1972). The arctic Caledonides and earlier oceans. *Geol. Mag.* 109 (4), 289–314. doi:10.1017/S0016756800037717

Hastie, A. R., Fitton, J. G., Kerr, A. C., McDonald, I., Schwindrofska, A., and Hoernle, K. (2016). The composition of mantle plumes and the deep Earth. *Earth Planet. Sci. Lett.* 444, 13–25. doi:10.1016/j.epsl.2016.03.023

Hawthorne, F. C., Oberti, R., Harlow, G. E., Maresch, W. V., Martin, R. F., Schumacher, J. C., et al. (2012). Nomenclature of the amphibole supergroup. *Am. Mineral.* 97 (11-12), 2031–2048. doi:10.2138/am.2012.4276

Hollocher, K., Robinson, P., Walsh, E., and Terry, M. P. (2007). The neoproterozoic ottfjället dike swarm of the Middle allochthon, traced geochemically into the scandian hinterland, western gneiss region, Norway. *Am. J. Sci.* 307, 901–953. doi:10.2475/06.2007.02

Hoskin, P. W. O., and Schaltegger, U. (2003). The composition of zircon and igneous and metamorphic petrogenesis. *Rev. Mineral. Geochem.* 53, 27–62. doi:10.2113/0530027

Jackson, S. E., Pearson, N. J., Griffin, W. L., and Belousova, E. A. (2004). The application of laser ablation-inductively coupled plasma-mass spectrometry to *in situ* U-Pb zircon geochronology. *Chem. Geol.* 211, 47–69. doi:10.1016/j.chemgeo.2004.06.017

Jakob, J., Alsaif, M., Corfu, F., and Andersen, T. B. (2017). Age and origin of thin discontinuous gneiss sheets in the distal domain of themagma-poor hyperextended pre-Caledonian margin of Baltica, southern Norway. *J. Geol. Soc.* 174 (3), 557–571. doi:10.1144/jgs2016-049

Jakob, J., Andersen, T. B., Mohn, G., Kjøll, H. J., and Beyssac, O. (2022). *Revised tectono-stratigraphic scheme for the Scandinavian Caledonides and its implications for our understanding of the Scandian orogeny*. The Geological Society of America. Special Paper 554. doi:10.1130/2022.2554(14)

Janák, M., Ravna, E. J. K., and Kullerud, K. (2012). Constraining peak P-T conditions in UHP eclogites: calculated phase equilibria in kyanite- and phengite-bearing eclogite of the Tromsø Nappe, Norway. *J. Metamorph. Geol.* 30, 377–396. doi:10.1111/j.1525-1314.2011.00971.x

Janák, M., Van Roermund, H., Majka, J., and Gee, D. (2013). UHP metamorphism recorded by kyanite-bearing eclogite in the Seve Nappe Complex of northern Jämtland, Swedish Caledonides. *Gondwana Res.* 23, 865–879. doi:10.1016/j.gr.2012.06.012

Kamo, S. L., Gower, C. F., and Krogh, T. E. (1989). Birthdate for the Iapetus Ocean? A precise U-Pb zircon and baddeleyite age for the Long Range dikes, southeast Labrador. *Geology* 17, 602–605. doi:10.1130/0091-7613(1989)017<0602:bftloa>2.3.co;2

Kamo, S. L., Krogh, T. E., and Kumarapeli, P. S. (1995). Age of the Grenville dyke swarm, Ontario–Quebec: implications for the timing of lapetan rifting. *Can. J. Earth Sci.* 32, 273–280. doi:10.1139/e95-022

Kelley, K. A., Kingsley, R., and Schilling, J.-G. (2013). Composition of plume-influenced mid-ocean ridge lavas and glasses from the mid-atlantic ridge, east pacific rise, galápagos spreading center, and gulf of aden. *Geophys. Geosystem* 14, 223–242. doi:10.1002/ggge.20049

Kirsch, M., and Svenningsen, O. M. (2016). Root zone of a continental rift: the neoproterozoic Kebnekaise intrusive Complex,northern Swedish Caledonides. *GFF* 138, 31–53. doi:10.1080/11035897.2015.1055298

Kjøll, H. J., Andersen, T. B., Corfu, F., Labrousse, L., Tegner, C., Abdelmalak, M. M., et al. (2019). Timing of breakup and thermal evolution of a pre-Caledonian Neoproterozoic exhumed magma-rich rifted margin. *Tectonics* 38, 1843–1862. doi:10.1029/2018TC005375

Klonowska, I., Janák, M., Majka, J., Froitzheim, N., and Kośmińska, K. (2016). Eclogite and garnet pyroxenite from stor jougdan, Seve nappe complex, Sweden: implications for UHP metamorphism of allochthons in the scandinavian Caledonides. *J. Metamorph. Geol.* 34, 103–119. doi:10.1111/jmg.12173

Klonowska, I., Janák, M., Majka, J., Petrík, I., Froitzheim, N., Gee, D. G., et al. (2017). Microdiamond on åreskutan confirms regional UHP metamorphism in the Seve nappe complex of the scandinavian Caledonides. *J. Metamorph. Geol.* 35, 541–564. doi:10.1111/jmg.12244

Kumpulainen, R. A., Hamilton, M. A., Söderlund, U., and Nystuen, J. P. (2016). "A new U-Pb baddeleyite age for the Ottfjället dolerite dyke swarm in the Scandinavian Caledonides-A minimum age for late Neoproterozoic glaciation in Baltica," in *Abstr. 32nd nordic geological winter meeting, Helsinki, Finland. Bulletin of the geological society of Finland, special volume*, 171–172.

Lanari, P., Vho, A., Bovay, T., Airaghi, L., and Centrella, S. (2019). Quantitative compositional mapping of mineral phases by electron probe micro-analyser. *Geol. Soc. Lond. Spec. Publ.* 478, 39–63. doi:10.1144/SP478.4

Majka, J., Rosén, Å., Janák, M., Froitzheim, N., Klonowska, I., Manecki, M., et al. (2014). Microdiamond discovered in the Seve nappe (scandinavian Caledonides) and its exhumation by the "vacuum-cleaner" mechanism. *Geology* 42, 1107–1110. doi:10.1130/G36108.1

McKerrow, W. S., and Ziegler, A. M. (1972). Palaeozoic Oceans. *Nat. Phys. Sci.* 240, 92–94. doi:10.1038/physci240092b0

Morimoto, N., Fabries, A. K., Ferguson, A. K., Ginzburg, I. V., Ross, M., Sefert, F. A., et al. (1988). Nomenclature of pyroxenes. *Am. Mineral.* 73, 1123–1133.

Paulsson, O., and Andréasson, P. G. (2002). Attempted break-up of Rodinia at 850 Ma: geochronological evidence from the seve–kalak superterrane, scandinavian Caledonides. *J. Geol. Soc. Lond.* 159, 751–761. doi:10.1144/0016-764901-156

Pearce, J. A. (2008). Geochemical fingerprinting of oceanic basalts with applications to ophiolite classification and the search for Archean oceanic crust. *Lithos* 100, 14–48. doi:10.1016/j.lithos.2007.06.016

Petrík, I., Janák, M., Klonowska, I., Majka, J., Froitzheim, N., Yoshida, K., et al. (2019). Monazite behaviour during metamorphic evolution of a diamond-bearing gneiss: a case study from the Seve nappe complex, scandinavian Caledonides. *J. Petrol.* 60, 1773–1796. doi:10.1093/petrology/egz051

Puffer, J. H. (2002). A Late Neoproterozoic eastern Laurentian superplume: location, size, chemical composition, and environmental impact. *Am. J. Sci.* 302, 1–27. doi:10.2475/ajs.302.1.1

Ridley, W. I. (2012). *Petrology of Associated Igneous Rocks. Volcanic massive sulfide occurrence model*. Reston, Virginia: U.S. Geological Survey.

Roberts, D. (1990). Geochemistry of malic dykes in the Corrovarre nappe, Troms, north Norway. *Nor. Geol. Unders. Bull.* 419, 45–53.

Roberts, D., Nordgulen, Ø., and Melezhik, V. (2007). The uppermost allochthon in the scandinavian Caledonides: from Laurentia ancestry through taconian orogeny to scandian crustal growth on Baltica. *Geol. Soc. Am. Mem.* 200, 357–373.

Root, D., and Corfu, F. (2012). U-Pb geochronology of two discrete Ordovician high-pressure metamorphic events in the Seve Nappe Complex, Scandinavian Caledonides. *Contrib. Mineral. Petrol.* 163, 769–788. doi:10.1007/s00410-011-0698-0

Rousku, S., Nääs, E., Barnes, C. J., Barker, A., and Majka, J. (2021). "Deciphering the Vássačorru igneous complex within the Seve nappe complex, scandinavian Caledonides," in *vEGU21, the 23rd EGU general assembly*.

Rubatto, D. (2017). Zircon: the metamorphic mineral. *Rev. Mineral. Geochem.* 83, 261–295. doi:10.2138/rmg.2017.83.9

Rudnick, R. L., and Gao, S. (2003). *Composition of the continental crust*, 3. Elsevier, 1–64. doi:10.1016/b0-08-043751-6/03016-4

Sawyer, E. W. (2001). Melt segregation in the continental crust: distribution and movement of melt in anatectic rocks. *J. Metamorph. Geol.* 19, 291–309. doi:10.1046/j.0263-4929.2000.00312.x

Schorn, S., and Diener, J. F. A. (2017). Details of the gabbro-to-eclogite transition determined from microtextures and calculated chemical potential relationships. *J. Metamorph. Geol.* 35, 55–75. doi:10.1111/jmg.12220

Sláma, J., Košler, J., Condon, D. J., Crowley, J. L., Gerdes, A., Hanchar, J. M., et al. (2008). Plešovice zircon-A new natural reference material for U–Pb and Hf isotopic microanalysis. *Chem. Geol.* 249, 1–35. doi:10.1016/j.chemgeo.2007.11.005

Stephens, M. B. (2020). Chapter 22 Upper and uppermost thrust sheets in the Caledonide orogen, Sweden: outboard oceanic and exotic continental terranes. In *Sweden: lithotectonic framework, tectonic evolution and mineral Resources*. Editors M. B. Stephens, and B. J. Weihed (Geological Society London Memoirs), 50, 549–575. doi:10.1144/M50-2019-12

Stephens, M. B., and Gee, D. G. (1989). *Terranes and polyphase accretionary history in the Scandinavian Caledonides*. Geological Society of America, 17–30. Special Paper 230.

Stølen, L. K. (1994). The rift-related mafic dyke complex of the Rohkunborri Nappe, Indre Troms, northern Norwegian Caledonides. *Nor. Geol. Tidsskr.* 74, 35–47.

Sun, S. S., and McDonough, W. F. (1989). Chemical and isotopic systematics of oceanic basalts: implications for mantle composition and processes. *Geol. Soc. Lond. Spec. Publ.* 42 (1), 313–345. doi:10.1144/gsl.sp.1989.042.01.19

Svenningsen, O. M. (1994). Tectonic significance of the meta-evaporitic magnesite and scapolite deposits in the Seve nappes, Sarek Mts., Swedish Caledonides. *Tectonophysics* 231 (1-3), 33–44. doi:10.1016/0040-1951(94)90119-8

Svenningsen, O. M. (2001). Onset of seafloor spreading in the Iapetus Ocean at 608 Ma: precise age of the Sarek dyke swarm, northern Swedish Caledonides. *Precambrian Res.* 110 (1-4), 241–254. doi:10.1016/s0301-9268(01)00189-9

Tegner, C., Andersen, T. B., Kjøll, H. J., Brown, E. L., Hagen-Peter, G., Corfu, F., et al. (2019). A mantle plume origin for the Scandinavian Dyke Complex: a 'piercing point' for 615 Ma plate reconstruction of Baltica? *Geochem. Geophys. Geosystems* 20, 1075–1094. doi:10.1029/2018GC007941

Thelander, T. (2009). *Bedrock map. In the Caledonides in northern Sweden, scale 1:250 000. Southern part*. Uppsala, Sweden: Sveriges Geolgiska Undersökning, 1–51.

Tilke, P. G. (1986). Caledonian structure, metamorphism, geochronology, and tectonics of the Sitas-Singis area, Sweden. Ph. D. thesis (Cambridge, MA: MIT), 295.

Vermeesch, P. (2018). IsoplotR: a free and open toolbox for geochronology. *Geosci. Front.* 9, 1479–1493. doi:10.1016/j.gsf.2018.04.001

Vernon, R. H. (2011). "Microstructures of melt-bearing regional metamorphic rocks," in *Origin and evolution of precambrian high-grade gneiss terranes, with special emphasis on the limpopo complex of southern africa*. Editors D. D. van Reenen, J. D. Kramers, S. McCourt, and L. L. Perchuk (Geological Society of America Memoir), 207, 1–11. doi:10.1130/2011.1207(01)

Walczak, K., Ziemniak, G., Barnes, C., Callegari, R., Bukała, M., Kielman-Schmitt, M., et al. (2022). Late neoproterozoic extended continental margin development recorded by the Seve nappe complex of the northern scandinavian Caledonides. *Lithos* 416-417, 106640–107417. doi:10.1016/j.lithos.2022.106640

Wang, K., Plank, T., Walker, J. D., and Smith, E. I. (2002). A mantle melting profile across the Basin and Range, SW USA. *J. Geophys. Res.* 107. doi:10.1029/2001jb000209

Wayte, G. J., Worden, R. H., Rubie, D. C., and Doop, G. T. R. (1989). A TEM study of disequilibrium plagioclase breakdown at high pressure: the role of infiltrating fluid. *Contrib. Mineral. Petrol.* 101, 426–437. doi:10.1007/bf00372216

Whitney, D. L., and Evans, B. W. (2010). Abbreviations for names of rock-forming minerals. *Am. Mineral.* 95, 185–187. doi:10.2138/am.2010.3371

Wiedenbeck, M., Hanchar, J. M., Peck, W. H., Sylvester, P., Valley, J., Whitehouse, M., et al. (2004). Further characterisation of the 91500 zircon crystal. *Geostand. Geoanalytical Res.* 28, 9–39. doi:10.1111/j.1751-908x.2004.tb01041.x

Wignall, P. B. (2001). Large igneous provinces and mass extinctions. *Earth-Science Rev.* 53, 1–33. doi:10.1016/s0012-8252(00)00037-4

Williams, H., and Hiscott, R. N. (1987). Definition of the lapetus rift-drift transition in western Newfoundland. *Geology* 15, 1044–1047. doi:10.1130/0091-7613(1987)15<1044:dotlrt>2.0.co;2

Zack, T., and John, T. (2007). An evaluation of reactive fluid flow and trace element mobility in subducting slabs. *Chem. Geol.* 239, 199–216. doi:10.1016/j.chemgeo.2006.10.020

Zwaan, K. B., and Van Roermund, H. (1990). A rift-related mafic dyke swarm in the Corrovarre Nappe of the Caledonian Middle Allochthon, Troms, North Norway, and its tectonometamorphic evolution. *Norges Geol. Unders. Bull.* 419, 25–44.